Research Paper

GEOSPHERE

GEOSPHERE; v. 11, no. 6

doi:10.1130/GES01154.1

11 figures; 3 tables; 1 supplemental file

CORRESPONDENCE: copeland@uh.edu

CITATION: Copeland, P., Bertrand, G., France-Lanord, C., and Sundell, K., 2015, $^{40}Ar/^{39}Ar$ ages of muscovites from modern Himalayan rivers: Himalayan evolution and the relative contribution of tectonics and climate: Geosphere, v. 11, no. 6, p. 1837–1859, doi:10.1130/GES01154.1.

Received 14 November 2014
Revision received 28 July 2015
Accepted 15 September 2015
Published online 23 October 2015

$^{40}Ar/^{39}Ar$ ages of muscovites from modern Himalayan rivers: Himalayan evolution and the relative contribution of tectonics and climate

Peter Copeland[1], Guillaume Bertrand[1,2,3,4], Christian France-Lanord[5], and Kurt Sundell[1]

[1]Department of Earth and Atmospheric Sciences, University of Houston, 3507 Cullen Boulevard, Houston, Texas 77204, USA
[2]Bureau de Recherches Géologiques et Minières (BRGM), Institut des Sciences de la Terre d'Orléans (ISTO), Unité Mixte de Recherche (UMR) 7327, 45060 Orléans, France
[3]Centre National de Recherche Scientifique (CNRS)/Institut National des Sciences de l'Univers (INSU), Institut des Sciences de la Terre d'Orléans (ISTO), Unité Mixte de Recherche (UMR) 7327, 45071 Orléans, France
[4]Université d'Orléans, Institut des Sciences de la Terre d'Orléans (ISTO), Unité Mixte de Recherche (UMR) 7327, 45071 Orléans, France
[5]Centre de Recherches Pétrograpiques et Géochimiques (CRPG), Centre National de Recherche Scientifique (CNRS), Université de Lorraine, 54501 Vandoeuvre les Nancy, Cedex, France

ABSTRACT

$^{40}Ar/^{39}Ar$ ages from detrital muscovites have been analyzed from six modern rivers in central and western Nepal; the size of the drainage basins associated with these samples ranges from a few square kilometers to >40,000 km^2. These data, when combined with previously published ages of detrital muscovites from other modern rivers in the region, suggest that a good correspondence between normalized age and normalized topography (the comparison of t^* and z^*) is rare, due to either nonuniform rates of passage through the ~400 °C isotherm or subsequent faulting in the drainage area. The closure temperature of Ar in muscovite is perhaps too high to make meaningful comparisons to modern topography in tectonic analysis of active orogens.

The distribution of $^{40}Ar/^{39}Ar$ ages from detrital muscovites from the Karnali basin in western Nepal is much older than that for the Narayani basin in central Nepal. The Karnali muscovites, when combined with previously published muscovites from the Siwalik Group in western Nepal and zircon fission track ages from modern and ancient samples from the region, suggest a thermal history for western Nepal consistent with vigorous tectonics (and attendant erosion) before the middle Miocene but a significant diminution in the rate of erosion since ca. 10 Ma.

$^{40}Ar/^{39}Ar$ ages of detrital muscovites from the Narayani basin in central Nepal suggest a markedly different history with an acceleration of the rate of erosion since ca. 10 Ma and reactivation of major faults; this is consistent with the abundant bedrock data from the Narayani basin.

The strong difference in the erosional history of the adjacent Karnali and Narayani basins, as evidenced by the $^{40}Ar/^{39}Ar$ ages from detrital muscovites, is not likely to have been due to variations in climate, but rather due to strain partitioning within the Himalaya during and after the Miocene.

INTRODUCTION

Much has been written regarding the relative importance of forces directed from below the surface of the Earth (tectonics) and forces directed from above the surface (erosion by rivers and glaciers) on the shaping of the landscape in active orogens (e.g., Burbank et al., 2003; Reiners et al., 2003; Gabet et al., 2008; Hodges et al., 2004; Whipple, 2009; Simon-Labric et al., 2014). Does one process dominate over the other, or do erosion, precipitation, and deformation work in compensatory ways? We present here $^{40}Ar/^{39}Ar$ ages from 10 samples from detrital muscovites from modern rivers in central and western Nepal that bear on this question.

To understand the data presented here, the geology of the Himalaya can be simplified as a series of north-dipping tectonostratigraphic units separated by faults. Starting in the north (higher elevation) and moving to the south (lower elevation), the geology can be described as follows (Fig. 1): (1) the Tethyan Sedimentary Sequence (TSS), a Paleozoic to Paleogene sedimentary sequence deposited on the Indian side of the Tethyan ocean; (2) the South Tibetan Detachment (STD), a fault with mostly normal displacement; (3) the Greater Himalaya Sequence (GHS), a series of kyanite- to sillimanite-grade gneisses variably intruded (usually near the top of the GHS) by Miocene High Himalayan leucogranites (HHG); (4) the Main Central Thrust (MCT); (5) the Lesser Himalayan Sequence (LHS), Precambrian to Mesozoic sedimentary rocks metamorphosed to low to medium grade; (6) the Main Boundary thrust (MBT); (7) the Miocene Siwalik Group, a 5–10-km-thick sequence of conglomerates, arkosic sandstones, and mudstones deposited in the Himalayan foreland basin; (8) the Main Frontal thrust (MFT); and (9) the Indo-Gangetic plain. The GHS, HHG, LHS, and Siwalik Group are muscovite rich. The major faults (STD, MCT, MBT, MFT) have had a complex structural evolution during Himalaya orogenesis with a broad pattern of the locus of deformation moving from north to south over

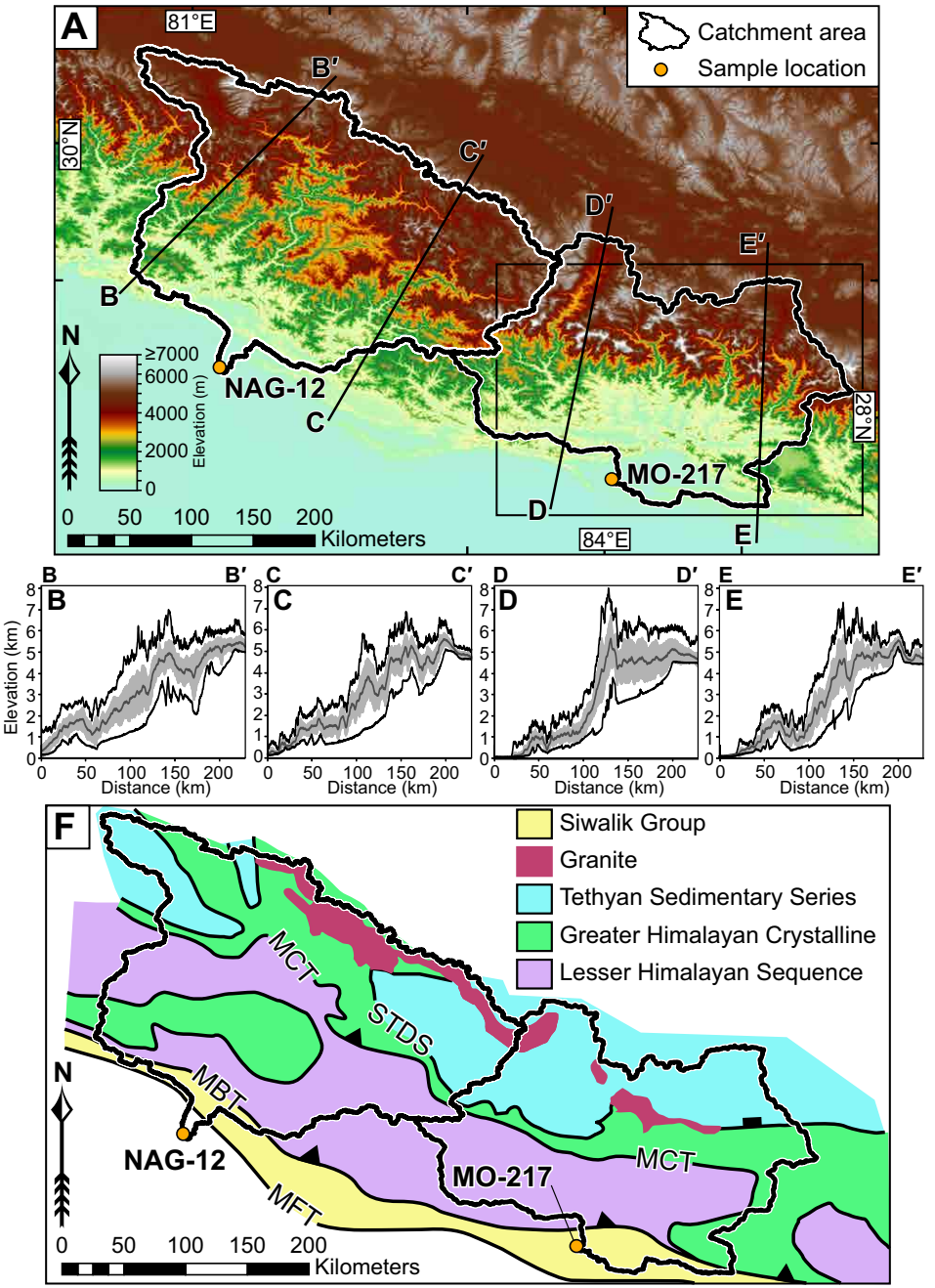

Figure 1. Location of field area, central Nepal. (A) Digital elevation model of the region. Black lines show catchment area for samples NAG-12 and MO-217. Black rectangle shows the extent of Figure 2. (B–E) Topographic profiles of the lines A-A′ through D-D′ in A. Profiles are calculated over a swath 25 km either side of the lines shown in a; the black lines show the average elevation and the gray area shows the range. (F) Geologic map of the region showing also the catchment areas for samples NAG-12 (Karnali) and MO-217 (Narayani). MBT—Main Boundary thrust; MCT—Main Central thrust; MFT—Main Frontal thrust; STDS—South Tibetan Detachment system.

time, but with many notable out-of-sequence exceptions (e.g., Schelling and Arita, 1991; Cattin and Avouac, 2000; DeCelles et al., 2001; Bollinger et al., 2004; Harrison et al., 1998; Hodges et al., 2004).

METHODS

Samples of modern river sand were obtained from 10 locations in central and western Nepal (Figs. 1 and 2). Nine samples were collected from the greater Narayani drainage basin in central Nepal varying in size from essentially the entire basin (>35,000 km^2) to high mountain locations of just a few square kilometers. Our final sample was collected from the Karnali River in western Nepal, where the river exits the Himalaya and enters the Gangetic plain (basin area ~46,000 km^2). Sample locations and the associated drainage basins of the sample with the largest catchments are shown in Figure 1; our samples with smaller drainage basins along with the location and drainage basins of similar samples from central Nepal previously reported (Brewer et al., 2003, 2006; Ruhl and Hodges, 2005) are shown in Figure 2.

Muscovite was separated from our sand samples by standard heavy liquid and magnetic methods. Samples were then sieved to 125–177 μm, 177–250 μm, and >333 μm (fine-, medium-, and coarse-grained, respectively). Samples were irradiated in four different batches at the Ford Nuclear Reactor at the University of Michigan following the procedures in Herman et al. (2010). Measured correction factors for interfering nuclear reactions for the individual irradiations are given in Part 1 of the Supplemental File[1].

The coarse-grained material (>333 μm) was heated using a CO_2 laser on individual grains; these grains were fused in a single step (Table 1; Supplemental File, Part 1); given the equipment used in this study it was not practical to analyze individual grains smaller than this. Fine-grained and medium-grained materials were step-heated in a double-vacuum resistance furnace in samples ranging from 3.5 to 6.0 mg (Table 1; Table A8 in the Supplemental File).

RESULTS

A summary of the ages from our samples is given in Table 1. Probability density diagrams and cumulative probability diagrams for single-crystal analysis are given in Figure 3, and age spectra diagrams for bulk samples of varying grain size are given in Figure 4. For the single-grain analyses, Table 2 lists the proportions of the largest subpopulation we are likely to have missed, given the number of grains analyzed and assuming various confidences, following the approach of Vermeesch (2004) and Andersen (2005); this analysis suggests

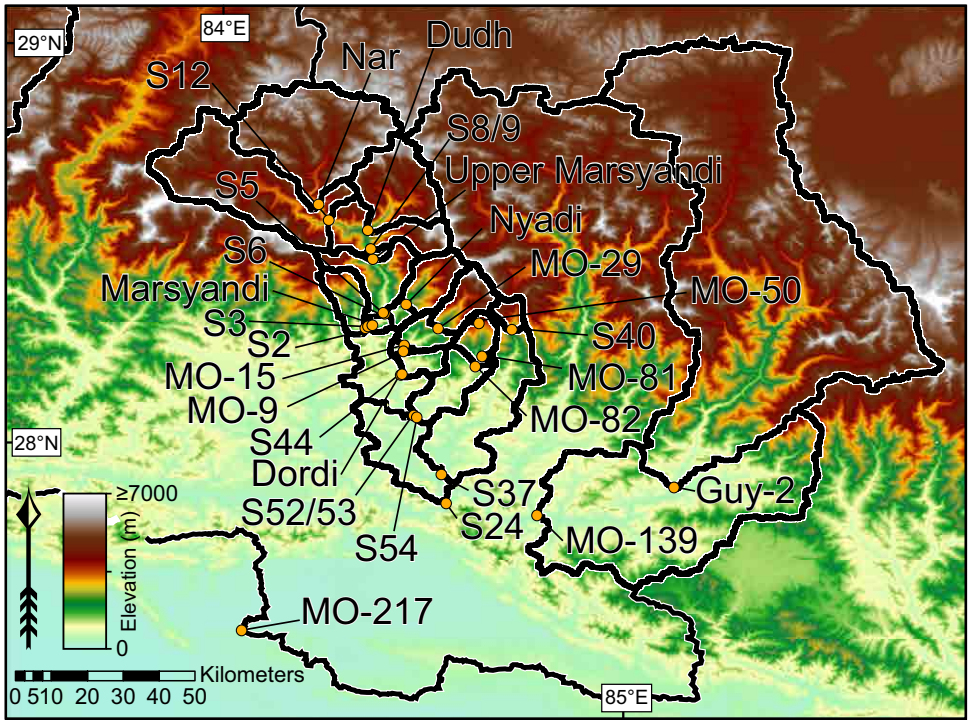

Figure 2. Location of samples and associated drainage basins from central Nepal (location shown in Fig. 1A).

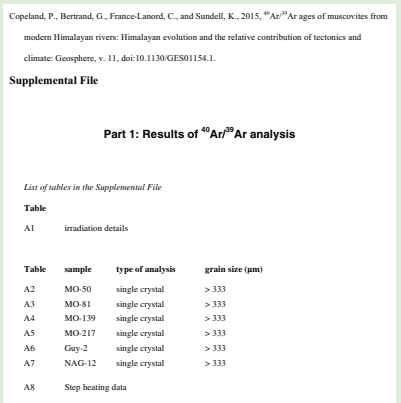

Copeland, P., Bertrand, G., France-Lanord, C., and Sundell, K., 2015, $^{40}Ar/^{39}Ar$ ages of muscovites from modern Himalayan rivers: Himalayan evolution and the relative contribution of tectonics and climate: Geosphere, v. 11, doi:10.1130/GES01154.1.

Supplemental File

Part 1: Results of $^{40}Ar/^{39}Ar$ analysis

List of tables in the Supplemental File

Table

A1 irradiation details

Table	sample	type of analysis	grain size (μm)
A2	MO-50	single crystal	> 333
A3	MO-81	single crystal	> 333
A4	MO-139	single crystal	> 333
A5	MO-217	single crystal	> 333
A6	Guy-2	single crystal	> 333
A7	NAG-12	single crystal	> 333

A8 Step heating data

[1]Supplemental File. Results of $^{40}Ar/^{39}Ar$ analysis and criteria for sample inclusion. Please visit http://dx.doi.org/10.1130/GES01154.S1 or the full-text article on www.gsapubs.org to view the Supplemental File.

TABLE 1. SUMMARY OF $^{40}Ar/^{39}Ar$ AGES FOR DETRITAL MUSCOVITES

Sample	Sample size (mg)	Grain size (μm)	Weighted average age (Ma)	Plateau age (Ma)	Integrated age (Ma)
Guy-2		>333	8.92 ± 0.05		
NAG-12	4.9	177–250		29.0 ± 3.0	112.4 ± 0.9
NAG-12		>333	15.85 ± 0.03		
MO-9	9.0	177–250		5.7 ± 0.1	5.7 ± 0.1
MO-15		177–250		5.6 ± 0.2	5.7 ± 0.1
MO-29		177–250		8.1 ± 0.1	12.8 ± 0.1
MO-50	4.6	125–177		7.1 ± 0.2	7.8 ± 0.2
MO-50	6.1	177–250		7.9 ± 0.6	8.0 ± 2.0
MO-50		>333	8.75 ± 0.04		
MO-81		>333	6.08 ± 0.02		
MO-82	6.5	177–250		6.8 ± 0.1	8.1 ± 1.4
MO-139	5.0	125–177		9.5 ± 0.8	15.0 ± 0.5
MO-139	5.8	177–250		11.6 ± 0.6	12.3 ± 0.3
MO-139		>333	10.60 ± 0.03		
MO-217	4.5	125–177		23.5 ± 0.7	28.1 ± 1.9
MO-217	3.5	177–250		22.0 ± 1.2	29.2 ± 0.5
MO-217		>333	9.98 ± 0.05		

that our samples are sufficient for a robust characterization of the range of ages of muscovites being eroded in these drainages.

In the following we discuss the data grouped geographically.

Dordi Khola

Three samples were collected from the Dordi Khola drainage, a left-bank tributary of the Marsyandi draining the LHS, GHS, and HHG (Fig. 2). Brewer et al. (2006) collected their sample S44 within the Lesser Himalaya from the confluence of the Dordi Khola and the Marsyandi River. Sample MO-9 was collected ~7 km upstream from S44, sample MO-15 was collected ~1.5 km upstream from MO-9, and sample MO-29 was collected ~10 km upstream from MO-15. MO-29 comes from an elevation of ~1450 m; the upper reaches of the Dordi Khola drainage include the peak Himalchuli (7893 m).

Each of these samples was analyzed only in bulk on the medium-grained fraction. The plateau ages for samples MO-9, MO-15, and MO-29 (going upstream) are 5.7 ± 0.1, 5.6 ± 0.2, and 8.1 ± 0.1, respectively (Fig. 4E). The final 30% gas released from MO-29 shows older ages, to ca. 20 Ma.

Chepe Khola

Three samples were collected from the Chepe Khola drainage. Sample MO-82 was collected within the Greater Himalaya, from ~25 km upstream from the confluence of Chepe Khola and the Marsyandi River, where Brewer et al. (2006) obtained their sample S-54. Sample MO-81, collected ~15 km north of the MCT, is from ~1 km up a small tributary of the main Chepe Khola drainage, ~3 km upstream from MO-82. Sample MO-50, collected from within the Greater Himalaya, comes from near the top of the Chepe Khola drainage, ~11 km upstream from MO-81. MO-50 comes from an elevation of ~3600 m, only 500–800 m below the drainage divide (between Chepe Khola and Dordi Khola) ~2 km to the west.

MO-82 was analyzed only in bulk (Fig. 4D). The plateau age (98% of the gas) of the medium multigrain samples is 6.8 ± 0.1 Ma (Table 1).

Single muscovites from sample MO-81 (n = 199) have a probability density plot with a very tight distribution (ca. 6 Ma; Fig. 3A); 25% of all grains are younger than 5.4 Ma, 50% of all grains are younger than 6.0 Ma, and 75% are younger than 6.7 Ma (Fig. 3E). The weighted average age of the single muscovites from MO-81 is 6.1 Ma (Table 1).

Single muscovites from sample MO-50 (n = 192) have a probability density plot with a broader distribution than MO-81 with a mode of ca. 9.1 Ma (Fig. 3A); 25% of all grains are younger than 5.9 Ma, 50% of all grains are younger than 8.3 Ma, and 75% are younger than 10.1 Ma (Fig. 3E). The weighted average age of the single muscovites from MO-139 is 8.8 Ma.

The plateau ages of the fine and medium multigrain samples are 7.1 ± 0.2 Ma and 7.9 ± 0.6 Ma, respectively (Table 1; Fig. 4C). The high-temperature steps from the age spectrum of the fine-grained material have ages to 15 Ma.

Trisuli River

Two samples (Guy-2 and MO-139) were analyzed from the Trisuli River; Guy-2 was collected near Trisuli Bazar and MO-139 was collected ~40 km downstream, just above the confluence of the Trisuli and the Bhuri Gandaki. Sample MO-217 (see following) was collected from the Narayani River ~60 km downstream from where the Trisuli and Kali Gandaki join to form the Narayani.

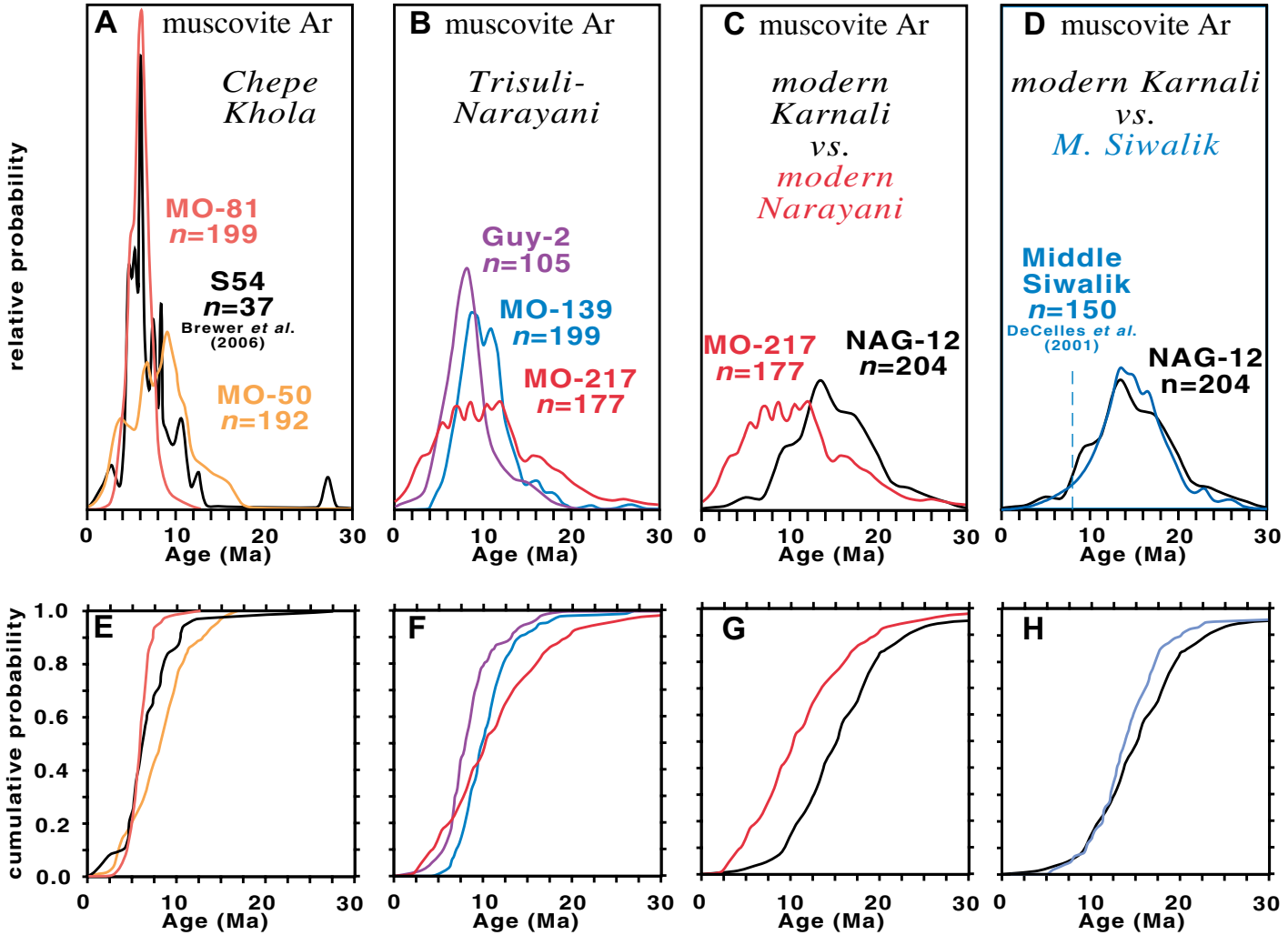

Figure 3. (A–D) Probability density functions for ages of detrital muscovites; all curves are normalized to have the same area. The dashed line in D represents the stratigraphic age of sample KZ-7 (DeCelles et al., 2001). (E–H) Cumulative probability plots corresponding to top panels (colors for sample identification).

Single muscovites from sample Guy-2 (n = 105) have a probability density plot with a peaked mode of ca. 8 Ma (Fig. 3B); 25% of all grains are younger than 6.8 Ma, 50% of all grains are younger than 8.2 Ma, and 75% are younger than 9.6 Ma (Fig. 3F). Only one grain has an age older than 18.1 Ma (540 Ma); when the one Paleozoic age is excluded, the weighted average age of the Guy-2 single crystals is 8.6 Ma (Table 1).

Single muscovites from sample MO-139 (n = 199) have a probability density function with 2 subequal modes ca. 8.5 and 10.5 Ma (Fig. 3B); 25% of all grains are younger than 8.4 Ma, 50% of all grains are younger than 10.0 Ma, and 75% are younger than 11.9 Ma (Fig. 3D). The weighted average age of the single muscovites from MO-139 is 10.7 Ma (Table 1).

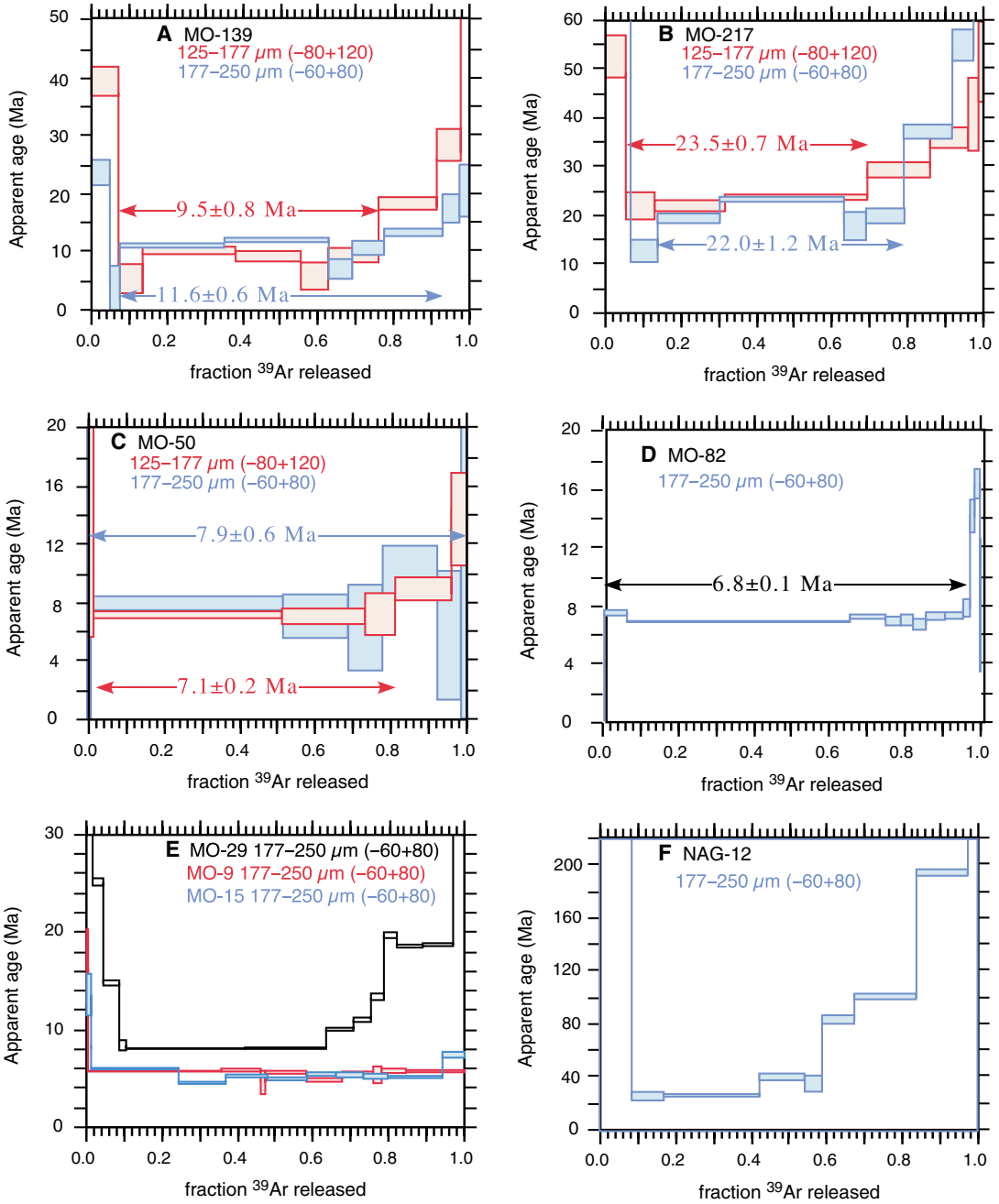

Figure 4. $^{40}Ar/^{39}Ar$ age spectra for bulk samples of detrital muscovites.

TABLE 2. MEASURE OF THE POTENTIAL FOR MISSING SUBPOPULATIONS

Sample	*n*	Vermeesch (2004) 95%	Vermeesch (2004) 98%	Andersen (2005) 95%
MO-50	192	3.2%	3.7%	1.5%
MO-81	199	3.3%	3.6%	1.5%
MO-139	199	3.2%	3.6%	1.5%
Guy-2	105	5.5%	6.2%	2.8%
MO-217	177	3.6%	4.0%	1.7%
NAG-12	204	3.2%	3.5%	1.5%

Note: Following the approach of Vermeesch (2004), the first column lists the largest subpopulation we are likely to have missed with a 95% confidence; the second column follows the same but with a 98% confidence. The less restrictive approach of Andersen (2005), given in the last column, suggests the detection limit (of a bin of any size) with 95% confidence.

The plateau ages of the fine and medium multigrain splits of MO-139 are 9.5 ± 0.8 Ma and 11.6 ± 0.6 Ma, respectively (Fig. 4A; Table 1).

Narayani River

Single muscovites from sample MO-217 (n = 177) have a probability density function with a broad mode, showing subequal representation for grains with ages from ca. 12 to 6 Ma (Fig. 3C); 25% of all grains are younger than 7.1 Ma, 50% of all grains are younger than 10.4 Ma, and 75% are younger than 14.8 Ma (Fig. 3G). The weighted average of the single crystal ages is 9.9 Ma (Table 1).

The plateau ages of the fine and medium multigrain splits of MO-217 are 23.5 ± 0.7 Ma and 22.0 ± 1.2 Ma (Fig. 4B; Table 1), respectively. In both age spectra, the high-temperature steps show older ages with the medium- and fine-grained fractions topping out ca. 40 and 55 Ma, respectively.

Karnali River

Single muscovites from sample NAG-12 (n = 204) have a probability density plot with a mode ca. 12.5 Ma (Figs. 3C, 3D); 25% of all grains are younger than 11.7 Ma, 50% of all grains are younger than 15.2 Ma, and 75% are younger than 18.7 Ma (Figs. 3G, 3H). The weighted average of the single crystal ages is 15.9 Ma (Table 1).

The medium-grained fraction of NAG-12 has an age spectrum from ~10% to 60% gas release having an age of ca. 29 Ma. After 60% release, ages climb to near 200 Ma (Fig. 4F).

DISCUSSION

Having data from large drainages and small drainages, from single crystals and bulk samples, and from coarse-grained and fine-grained material, we have the opportunity for a variety of comparisons in our discussion of these data.

Variation of Age with Grain Size

Of our 10 samples, we analyzed 2 size fractions from 1 sample (NAG-12) and 3 size fractions from 3 other samples (MO-50, MO-139, and MO-217). For samples MO-50, MO-139, and MO-217, the plateau ages for the bulk analysis of the fine grained (125–177 μm) and medium grained (177–250 μm) are within a few percent of each other (Fig. 5). In two of these samples, MO-50 and MO-139, the average of the ages of the single-crystals (>333 μm) are similar to the plateau ages of the two smaller grain sizes analyzed in bulk. In contrast, samples MO-217 and NAG-12 have the average of the single-crystal analyses significantly younger than the plateau age of the medium-grained bulk analysis.

Samples MO-217 and NAG-12 represent areas with a greater proportion of LHS rocks than samples MO-50 and MO-139. Given that the LHS is more likely to contain muscovites with a pre-Himalayan age (e.g., Copeland et al., 1991; Wobus et al., 2005; Johnson and Rogers, 1997), it is not surprising that the samples with the greater proportion of LHS in the catchment are the samples with the greatest age difference between grain sizes.

It is tempting to suggest that the finest grained muscovites analyzed here should have the lowest closure temperature and the coarsest muscovites have the highest closure temperature, but we cannot say that material we have today is in the same condition it was when it was last at 400 °C; the smaller grains may be smaller because of recent sedimentary action in the modern rivers and therefore unrelated to the conditions at Ar closure. Moreover, in the three samples (MO-50, MO-139, and MO-217) where we have analyses from our small, medium, and large fractions, there is no simple relationship between bulk or average age and grain size. For sample MO-217, the relationship is opposite from what one would predict if grain size were the only factor determining the age of these muscovites (Fig. 5).

Single-Grain Data

Age Distributions

Our new samples (in combination with previously published data) contain muscovites derived from basins with widely varying sizes. Sample NAG-12 contains material that possibly comes from the entire drainage basin of the Karnali River, ~46,160 km^2. Sample MO-217 contains muscovites that came from an area of ~35,338 km^2, essentially all of the Narayani basin (which is made up of several tributaries, including the Kali Gandaki, the Marsyandi, the Burhi Gandaki, and the Trisuli). Some other relevant detrital geochronology data have been published for the Karnali basin (see following), but we first discuss the MO-217 and several samples from smaller parts of the same basin (our samples MO-9, MO-15, MO-29, MO-50, MO-81, MO-82, MO-139, and Guy-2, and samples from Brewer et al., 2003, 2006; Ruhl and Hodges, 2005; other samples were selected because of the spatial overlap of some of our samples). We start with the new data reported here from small drainages and work toward the larger drainages. We then compare our data to the previously

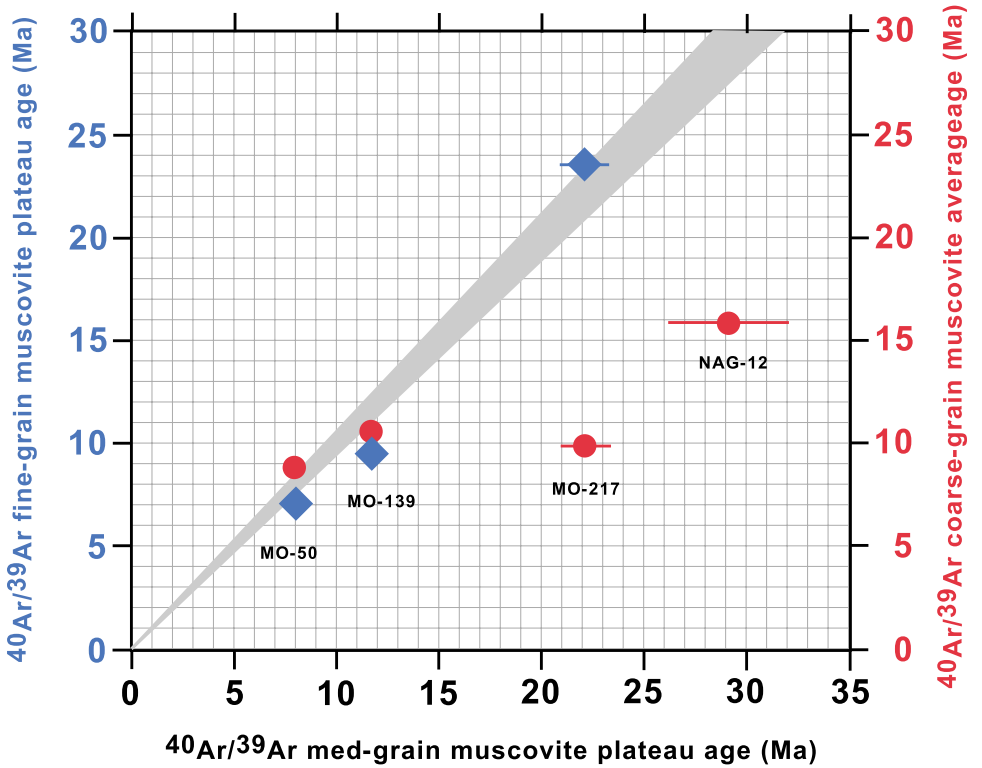

Figure 5. Comparison of plateau ages for fine-grained and medium-grained bulk samples and average age of individual ages of coarse-grained material for detrital muscovites. Gray band represents the 1:1 line with an uncertainty of ±5%.

published $^{40}Ar/^{39}Ar$ ages from detrital muscovites from the region (Brewer et al. 2003, 2006; Ruhl and Hodges, 2005).

Chepe Khola and Dordi Khola are small drainages (~309 and 352 km^2, respectively). Brewer et al. (2003, 2006) reported $^{40}Ar/^{39}Ar$ ages for detrital muscovites collected from the modern river sediment in the Chepe and Dordi Kholas, just above the confluences with the Marsyandi.

The two samples most relevant to our data from Brewer et al. (2003, 2006) have $n = 37$ and $n = 39$. Therefore, although we can be generally sure that we have not missed small subpopulations (<3%–4%) when n is near 200, note that with $n = 37$, the detection limit at 95% confidence is 7.8% of the total (Andersen, 2005). Nonetheless, we can make some interesting comparisons between our data and previously published data.

If the catchment had uniform erosion rates during the time the muscovites in the basin were closing to Ar loss, and the sampling of detrital muscovites is representative of the muscovites found in the bedrock of the catchment (see Ruhl and Hodges, 2005), the distribution of ages should become older and more tightly grouped as the elevation of sample sites increases and the relief of the associated drainage decreases. In Chepe Khola, this is not what is observed.

Sample MO-50 comes from near the top of the Chepe drainage (z_{min} = 3736 m, z_{max} = 4500 m, where z is elevation above sea level; area = 2 km^2). MO-81 also represents a small drainage on the side of the main Chepe drainage (z_{min} = 1625 m, z_{max} = 2961 m; area = 4 km^2); MO-82, which is from very near MO-81, has a bulk age for the 177–250 µm grains of 6.8 ± 0.1 Ma (Table 1), indicating no fractionation for age in grain size in this drainage. Sample S54 of Brewer et al. (2006) comes from the bottom of the drainage (z_{min} = 452 m, z_{max} = 4958 m; area = 309 km^2).

The distribution of detrital muscovite ages from MO-50 is slightly older (mode and average age of 9.1 Ma and 8.8 Ma, respectively) than for samples MO-81 (6.1 and 6.1 Ma) and S54 (6.1 and 7.6 Ma) but MO-50 has the widest distribution, with ages ranging from 1.4 ± 0.2 to 16.4 ± 1.9 Ma. MO-50 comes from almost the highest portion of the Chepe drainage and from a very small area of <2 km^2; both of these observations would lead one to predict a very narrow age distribution for the muscovites in this sample. Reasons that this is not the case could be that the top of this ridge has had glacial deposits (the modern glaciers of the Annapurna range are just a few kilometers away), or wind-blown deposits that are not present in lower elevations (bringing extra-

basinal muscovites), or the drainage basin of sample MO-50 has a structural complexity not in proportion to its area. Similar arguments may explain the poor correspondence between the distribution of ages and hypsometry for MO-81 (see following); however, MO-81 has a very narrow range of ages with 95% of all grains between 3.8 and 8.8 Ma.

We have no single-crystal data from Dordi Khola (the drainage immediately adjacent to Chepe Khola to the northwest), but we can compare the single-crystal data of sample S44 of Brewer et al. (2006), taken from where Dordi Khola joins the Marsyandi River. The range in muscovite ages in S44 (n = 39) is 2.6–12.8 Ma with an average of 5.7 Ma. Our bulk samples (all 177–250 µm), MO-9, MO-15, and MO-29, going upstream, have plateau ages of 5.7, 5.6, and 8.1 Ma, respectively. This, along with the generally good correspondence between t* and z* (normalized age and normalized topography, respectively) for sample S44 (see following) suggests that the structural complexities in Dordi Khola are less than in the adjacent Chepe Khola. However, it is possible that our step-heating data from samples MO-9, MO-15, and MO-29 obscure details that might have been better understood with single-crystal data.

We have single-crystal data from two samples along the Trisuli River. The more-upstream sample, Guy-2 (area 4740 km^2), has a younger and narrower distribution of muscovite ages than sample MO-139, collected near where the Trisuli and Marsyandi merge (area 6597 km^2).

Our two samples that represent large drainages, NAG-12 from the Karnali basin (46,160 km^2) and MO-217 from the Narayani basin (35,338 km^2), have very different age distributions (Fig. 3C). We discuss the significance of this difference herein; next we compare the distributions of ages and hypsometry for these two samples, our 4 additional samples, and 18 similar samples from central Nepal (previously reported; Brewer et al. 2003, 2006; Ruhl and Hodges, 2005).

Relationship between Age Distribution and Hypsometry

Ruhl and Hodges (2005) presented an approach in which a comparison of a distribution of cooling ages from a modern detrital sample can be made to the hypsometry of the basin represented by the detrital sample. This analysis requires several assumptions: (1) the region has not been tilted since the rocks now present at the surface passed through the closure isotherm, and no significant faulting occurred within the drainage basin to modify the relative position of the rocks in question since mineral closure; (2) the rate of erosion was uniform across the drainage basin in the interval during which the minerals analyzed passed through their closure interval; and (3) the detrital material faithfully samples the bedrock in the catchment (in the current example, we need to consider if all the rocks at the surface of the drainage basin today contain muscovite in about the same proportion). Ruhl and Hodges (2005) suggested that if these assumptions were valid, the distribution of detrital ages should mimic the distribution of elevation in a drainage basin; that is, the lack of correspondence between these two distributions would be cause to doubt the validity of the assumptions.

However, how does one compare a distribution of ages to a distribution of elevations? Ruhl and Hodges (2005) proposed a method for dealing with this problem, which we follow with modifications. In order to meaningfully compare these different distributions, each must be nondimensionalized. To do so, we transform each measured age, t, and each elevation point, z, using the following:

$$t^* = \frac{t - t_{min}}{t_{max} - t_{min}}, \quad (1)$$

and

$$z^* = \frac{z - z_{min}}{z_{max} - z_{min}}. \quad (2)$$

When t* and z* are each plotted as cumulative distribution function (CDF) they are comparable. However, because we can obtain a digital elevation model for a particular catchment that may contain thousands to millions of elevation points and any distribution of ages of detrital minerals will be made up of perhaps as few as dozens to usually no more than hundreds of analyses, it still is not fair to compare these distributions of very different size, assuming that the ages are a reflection of the topography. Ruhl and Hodges (2005) chose to deal with this problem by randomly sampling their z* distribution 300 times with n equal to the number of detrital grains analyzed from the drainage. We chose a different, but perhaps statistically equivalent, approach of sampling the topography and then normalizing as above; the details of our procedure are given in Part 2 of the Supplemental File. This family of sample z* curves are then compared to the t* curve.

To compare the t* and z* curves for each sample, we first applied the two-sample Kolmogorov-Smirnov (K-S) test and the two-sample Kuiper test. The Kuiper test is a variant of the two-sample K-S test that ensures equal sensitivity for all x values in a given test, while the K-S test is more sensitive to the median. The k value of the K-S test is the maximum difference in cumulative probability for all points on the two distributions. The v value is the k value equivalent of the Kuiper test, the only difference is that it is the sum of the maximum distance between one CDF above and below the other. In both cases, smaller values (v or k) suggest that the distributions are more similar. Resulting p values from both tests address the question, what is the probability that the two cumulative frequency distributions would be as far apart as observed (the k value and v value) if the two samples were randomly sampled from identical populations?

Both tests gave similar results (Table 3); however, a qualitative assessment of p value against visual inspection of each of the t*-z* plots suggests that neither measure is adequate. For example, sample MO-50 gives a p value for both the K-S and Kuiper tests of 0.000, suggesting that they are dissimilar, although a visual inspection of the t*-z* plot suggests otherwise, as they are obviously more similar than other t*-z* comparisons that yielded higher p values (e.g., sample S3, Fig. 6N). This is likely because these types of tests are pass-fail hypothesis tests, and not strictly a measure of similarity. Furthermore, these tests do not work well for dimensionless distributions (as noted by Ruhl and Hodges, 2005), and both tests are highly dependent on n with higher n typically yielding lower p values (see Table 3).

TABLE 3. STATISTICS OF DRAINAGE

	Area (km²)	Min Elev (m)	Max Elev (m)	Relief	*n*	Kuiper Test (CDF) mean *p*	Kuiper Test (CDF) std *p*	Kuiper Test (CDF) mean *v*	Kuiper Test (CDF) std *v*	K-S Test (CDF) mean *p*	K-S Test (CDF) std *p*	K-S Test (CDF) mean *k*	K-S Test (CDF) std *k*	Cross Corr. (CDF) mean	Cross Corr. (CDF) std	Cross Corr. (CDF) mean	Cross Corr. (CDF) std	Likeness (PDF) mean	Likeness (PDF) std
Muscovite																			
MO50	2	3736	4500	764	192	0.00	0.00	0.32	0.04	0.00	0.00	0.30	0.04	0.95	0.01	0.49	0.11	0.74	0.03
MO81	4	1625	2961	1336	199	0.00	0.00	0.52	0.04	0.00	0.00	0.48	0.04	0.91	0.02	0.23	0.09	0.56	0.04
MO139	6597	329	7362	7033	195	0.00	0.00	0.56	0.03	0.00	0.00	0.46	0.04	0.81	0.02	0.04	0.03	0.51	0.03
MO217	35338	129	8143	8014	168	0.00	0.00	0.33	0.04	0.00	0.01	0.22	0.04	0.95	0.01	0.33	0.10	0.73	0.03
NAG12	46160	129	7707	7578	189	0.00	0.00	0.31	0.05	0.00	0.01	0.22	0.03	0.95	0.01	0.52	0.12	0.75	0.04
GUY2	4740	488	7362	6874	104	0.00	0.00	0.59	0.04	0.00	0.00	0.56	0.05	0.75	0.03	0.02	0.03	0.48	0.05
Dudh	389	1997	7673	5676	92	0.10	0.15	0.27	0.06	0.21	0.20	0.17	0.05	0.96	0.02	0.65	0.12	0.80	0.05
Nar	825	2874	7096	4222	99	0.01	0.04	0.34	0.06	0.03	0.08	0.27	0.08	0.93	0.02	0.77	0.14	0.76	0.07
Marsy.	2776	817	8055	7238	295	0.00	0.00	0.47	0.03	0.00	0.00	0.42	0.03	0.83	0.02	0.11	0.04	0.60	0.02
Nyadi	180	1369	7473	6104	96	0.41	0.33	0.19	0.06	0.39	0.32	0.15	0.06	0.98	0.01	0.88	0.10	0.88	0.05
U. Mars	2299	1491	8055	6564	35	0.03	0.08	0.53	0.11	0.01	0.04	0.52	0.12	0.79	0.05	0.31	0.25	0.56	0.12
Dordi	353	565	7827	7262	38	0.01	0.04	0.49	0.07	0.08	0.10	0.31	0.06	0.83	0.04	0.48	0.18	0.66	0.06
S2	136	810	4958	4148	24	0.37	0.24	0.37	0.07	0.31	0.26	0.29	0.08	0.93	0.02	0.41	0.22	0.75	0.07
S3	2781	799	8055	7256	44	0.02	0.04	0.47	0.08	0.08	0.08	0.28	0.05	0.87	0.04	0.15	0.13	0.63	0.08
S5	215	946	7473	6527	32	0.53	0.29	0.29	0.06	0.43	0.31	0.23	0.07	0.95	0.02	0.58	0.20	0.79	0.06
S6	2540	918	8055	7137	49	0.01	0.03	0.47	0.07	0.02	0.07	0.37	0.08	0.91	0.04	0.18	0.19	0.62	0.08
S8+S9	2282	1667	8055	6388	45	0.01	0.06	0.53	0.11	0.00	0.02	0.52	0.12	0.84	0.05	0.21	0.22	0.53	0.12
S12	1627	2565	7924	5359	25	0.39	0.32	0.37	0.10	0.40	0.31	0.27	0.09	0.90	0.04	0.49	0.24	0.73	0.08
S24	4790	233	8055	7822	64	0.00	0.00	0.45	0.06	0.00	0.00	0.43	0.06	0.84	0.04	0.14	0.13	0.61	0.06
S37	608	313	6060	5747	22	0.24	0.21	0.48	0.09	0.26	0.21	0.31	0.08	0.77	0.09	0.71	0.15	0.72	0.07
S40	55	2048	6060	4012	20	0.60	0.31	0.34	0.09	0.48	0.33	0.27	0.09	0.93	0.04	0.39	0.23	0.75	0.07
S44	352	580	7827	7247	38	0.01	0.04	0.49	0.07	0.08	0.10	0.31	0.06	0.83	0.04	0.45	0.19	0.65	0.06
S52+S53	3544	441	8055	7614	31	0.01	0.03	0.51	0.06	0.08	0.12	0.36	0.08	0.75	0.06	0.05	0.07	0.56	0.06
S54	309	452	4958	4506	35	0.05	0.10	0.45	0.07	0.03	0.08	0.39	0.08	0.94	0.02	0.24	0.17	0.66	0.07
Apatite																			
MAR6	11696	297	8042	7745	32	0.02	0.04	0.52	0.08	0.02	0.06	0.44	0.09	0.89	0.03	0.06	0.10	0.58	0.08
MAR10	4784	260	8055	7795	54	0.00	0.00	0.52	0.06	0.00	0.00	0.44	0.07	0.77	0.05	0.13	0.13	0.58	0.06
KAR	46160	129	7707	7578	25	0.07	0.11	0.49	0.08	0.02	0.04	0.47	0.08	0.79	0.07	0.10	0.13	0.55	0.07

An alternative approach to measure similarity between CDF curves is to calculate the correlation coefficient (r^2) for each of the z^* CDFs with their corresponding t^* CDFs. If the assumptions of Ruhl and Hodges (2005) are met, a regression line of t^* versus z^* CDFs would give an r^2 value close to 1. This calculation resulted in mean r^2 values between 0.75 and 0.97, the former being very dissimilar (see samples Dudh and S52–53, Fig. 6W) and the latter being very similar (see Nyadi, Fig. 6J). This range is expected to be low, as CDFs are always monotonically increasing, but is no less meaningful in its description of similarity. For example, for sample MO-50, the normalized hypsometric curves versus normalized ages appear to be very similar, and the r^2 suggests the same. This approach also gives relatively low standard deviations compared to the K-S and Kuiper tests, and is not as dependent on *n*.

We investigated two other measures of similarity, but instead of between CDF curves, between normalized probability density plots (PDPs). A PDP, as typically used in geological literature, is a type density estimate that uses the analytical uncertainty as the sample bandwidth in constructing individual Gaussian kernels that are summed and normalized to give relative probability. Because t^* and z^* are dimensionless, we used a constant (6%) bandwidth for individual t^* and z^* kernels along an x range of –0.2 and 1.2 to construct the PDPs, with the additional space on the ends to account for the tails of the distributions. For the same t^* and z^* distributions, we calculated the r^2 values and the likeness value between PDPs (see Satkoski et al., 2013, for explanation of likeness). Results show the same general trend in similarity to those for r^2 values between CDF curves (Fig. 7).

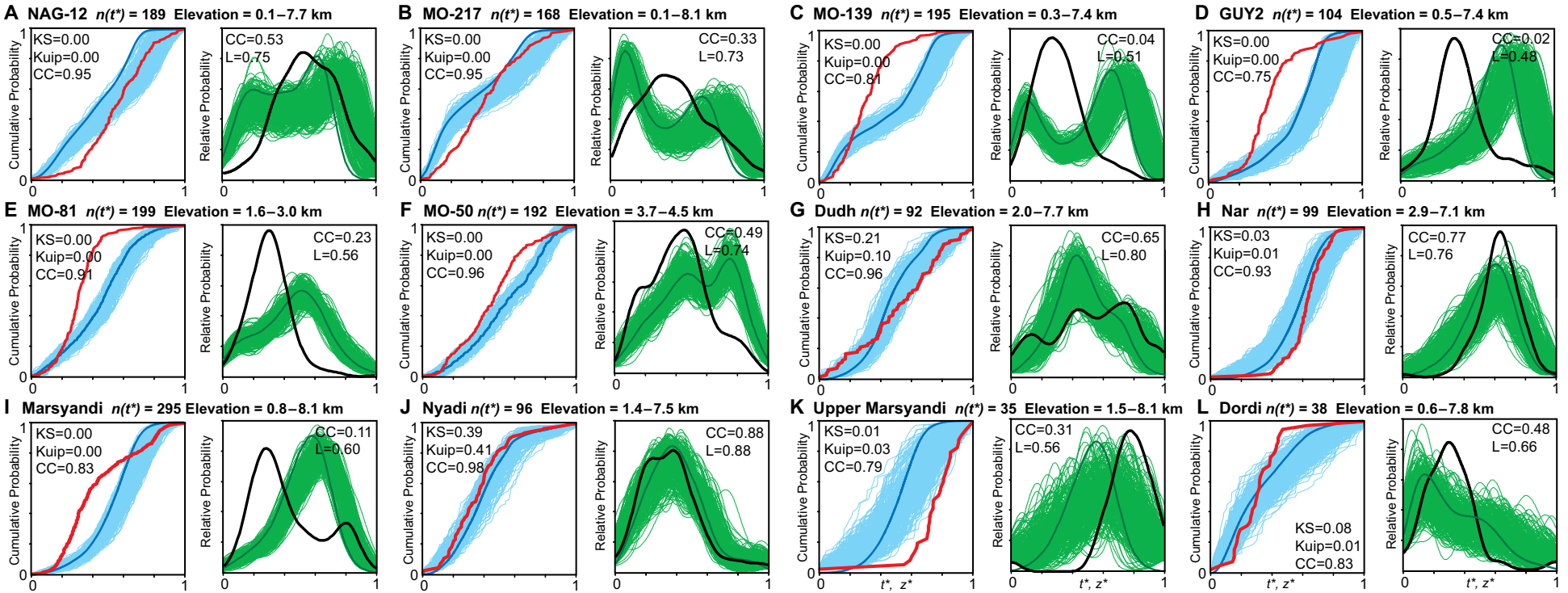

Figure 6 (*on this and following page*). Comparison of *t and *z** (normalized age and normalized topography, respectively) distributions for samples of muscovites from modern rivers from this study as well as similar data previously reported from other samples in central Nepal (Ruhl and Hodges, 2005; Brewer et al., 2003, 2006). Red and black curves are *t** in cumulative distribution functions (CDF) and probability density plots (PDP), respectively. Dark blue and dark green curves are *z** calculated from the complete digital elevation model (DEM) data for the drainage basin associated with each sample for CDF and PDP, respectively. Light blue lines are *z** calculated based on a subset of the DEM data produced by randomly sampling 300 times the elevations of the basin with *n* equal to the number of samples used to construct *t** for CDF and PDP, respectively. Sample numbers are shown. KS—Kolmogorov-Smirnov test; Kuip—Kuiper test. CC—Cross correlation coefficient. L—Likeness. See text for details.**

Table 3 lists geographic details of each drainage basin along with the mean and standard deviation of the *p* values (K-S and Kuiper tests of CDFs), *k* values (K-S test of CDFs), *v* values (Kuiper test of CDFs), r^2 values (of CDFs), r^2 values (of PDPs), and likeness values (of PDPs) for the 300 *t**-*z** comparisons of each sample. The 24 samples shown in Figure 6 represent a large geographic variety of drainage basins. The areas of these catchments vary from 2 to 46,160 km^2, and the relief varies by more than a factor of 10. Given the restrictions of the assumptions of Ruhl and Hodges (2005) associated with the comparison of *t** and *z** distributions, one would expect smaller catchments to be more likely to have a good correspondence between *t** and *z**. The larger a region, the more likely variations in structural history or rock type (in this case, muscovite-poor rocks) would lead to a divergence between *t** and *z**. However, there is no significant relationship between *t**-*z** statistical comparisons given in Table 3 and any geographic parameters of the basins except for drainage basin area, and this is only if the largest two catchments are not considered (Fig. 7). Even if we restrict our analysis to basins with areas <1000 km^2, the relationship between geographic characteristics and any of the statistical indices of the similarity between *t** and *z** is not strong.

In any rigorous sense, only extreme data filtering will allow even a modest trend between any of the geographic descriptions and the statistical comparisons of *t** and *z** given in Table 3 to emerge. This suggests that for $^{40}Ar/^{39}Ar$ dates from muscovite, the several assumptions of Ruhl and Hodges (2005) concerning tectonism during and after Ar closure are unlikely to have been satisfied.

The expectation that *t** and *z** might have some systematic covariation is an extension of the often-used age versus elevation approach used in many studies. In these works, samples are collected from a transect across a short distance (the shorter and the steeper the better) and cooling ages are compared with elevation to determine erosion rates. The same assumptions concerning structural complexity listed here for large basins are needed in these sorts of studies. Some such studies (e.g., Copeland et al., 1987) have found

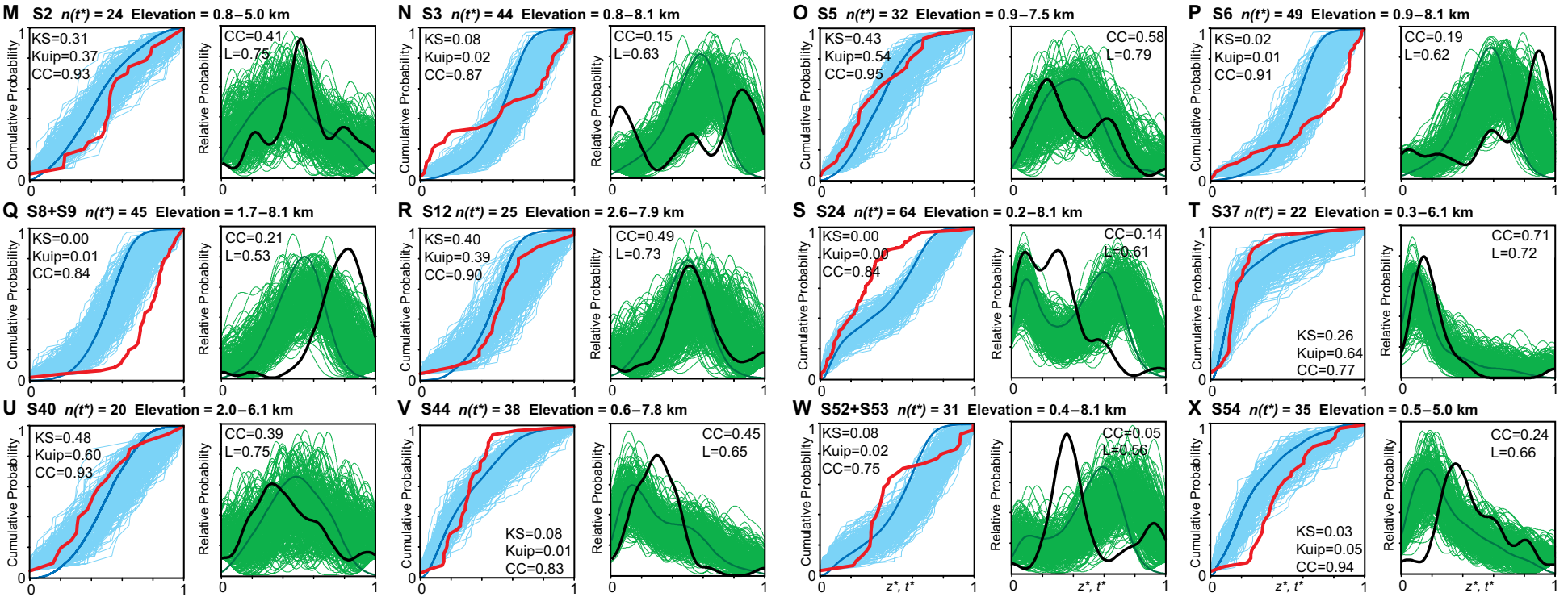

Figure 6 (*continued*).

evidence that these assumptions apply to relatively high closure temperature, T_c, thermochronologic systems such as $^{40}Ar/^{39}Ar$ ages from biotite (T_c ~350–300 °C, McDougall and Harrison, 1999), but the assumptions that need to be applied are needed within a much smaller area (i.e., along the line of traverse rather than over an entire drainage basin).

It seems that the poor correspondence between t^* and z^* for most of the samples discussed here from large drainage basins is mostly due to the rather high T_c of Ar in muscovite of ~400 °C (Harrison et al., 2009). Assuming geothermal gradients in the range of 22–30 °C/km, between 13 and 18 km of erosion must take place to bring a muscovite in a metamorphic rock to the surface after it has cooled below the T_c of Ar. Even at Himalayan rates of erosion, this allows ample time for structural displacement that would produce the kind of t^*-z^* relationships in Figure 6 and Table 3.

Therefore, although it may sometimes be possible to observe a strong correlation between muscovite $^{40}Ar/^{39}Ar$ ages and elevation along a transect of a few kilometers (e.g., Huntington et al., 2006), the structural variability likely to be present across an entire drainage basin will invalidate the assumptions necessary to allow meaningful comparisons of t^* and z^*. This is illustrated well in the work of Herman et al. (2010), which at the time of this writing is the most detailed inventory of bedrock muscovite $^{40}Ar/^{39}Ar$ ages over a large area in the Himalaya. In this study, in the Kathmandu region, there is a strong correlation of muscovite ages with geologic structures and very little region-wide variation with elevation. The results given in Table 3 and Figure 6 suggest that the threshold for the size of the drainage basin beyond which it is imprudent to expect the necessary assumptions for age-elevation studies to hold is rather small. We see poor correspondence between of t^* and z^* for basins as small as a few square kilometers, a few hundred square kilometers, and anything larger than an area equal to a circle with radius of ~23 km. However, 5 of the smallest 13 basins in Table 3 and Figure 6 have relatively good statistical matches between t^* and z^*.

The problem of a nonuniform distribution of muscovite-poor rocks (e.g., pure marble) would only exacerbate the mismatch between t^* and z^*. This may not be a problem for the samples from small basins, but the samples discussed here with large basins that include substantial proportions of the LHS may be not well sampled by the coarse muscovites used in most detrital studies. As discussed here, the technical necessity of restricting single-crystal analysis to coarse-grained muscovites (which are less common in the LHS in our observation) will bias the population toward the GHS and away from the LHS.

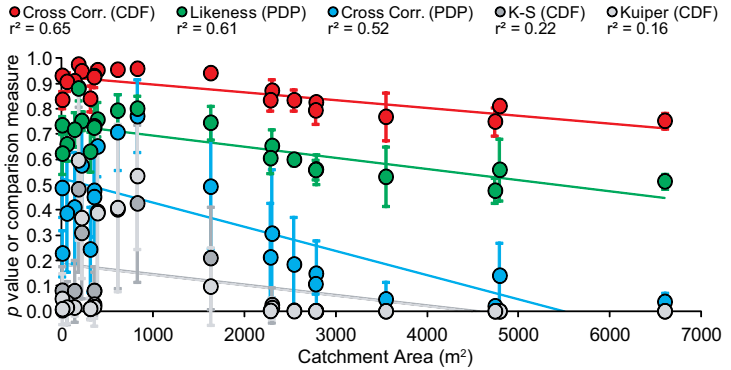

Figure 7. Comparison of the statistical tests of *t versus *z** (normalized age and normalized topography, respectively) (Fig. 6) plotted against catchment area. Corr.—correlation; CDF—cumulative distribution function; PDP—probability density plot; K-S—Kolmogorov-Smirnov.**

Although the statistical analysis of Table 3 suggests that only a few of the basins discussed here come close to a rigorous definition of a good fit between the distribution of elevation and muscovite ages, an inspection of Figure 6 shows that some fits are clearly better than others. Figure 6 offers a bootstrap confidence assessment by qualitatively checking how well the *t** overlaps with the cloud produced by the 300 random samplings of the topography. The samples with the best statistics in Table 3 have a relatively good fit using this measure (samples Nar, Nyadi, S5, S12, and S37). The basins corresponding to these samples have areas that range from 180 to 1627 km^2. One might expect this relationship to get worse with increasing basin area, but this is not the case, particularly for the six new samples reported here. The two samples from very small catchments (MO-50 and MO-81) fail the bootstrap measure of overlap over most of the range of *t** and *z**, but the two largest basins (corresponding to NAG-12 and MO-217) have *t** that overlaps with the *z** cloud about ¾ of the distribution for the CDF but do not overlap nearly as well for the PDP (Figs. 6A, 6B). The two medium-sized basins (Guy-2 and MO-139) have the worst correspondence (Figs. 6C, 6D). Rather than suggesting that the assumptions of Ruhl and Hodges (2005) are met better for big basins than for small, the better fit of *z** and *t** for the largest basins suggests an averaging over space (in particular over a range of elevations) and time not possible in small basins (see Gabet et al., 2008).

The overall poor correspondence between *t** based on muscovite ages and *z** in central Nepal suggests that the cooling from ~400 °C to surface temperatures requires so much time (even at Himalayan erosion rates) that post–muscovite closure deformation of the region (even relatively small regions) will be a much stronger factor in the geographic distribution of muscovite ages than a simple age-elevation relationship. However, *t** distributions based on other thermochronometers with lower closure temperatures such as zircon or apatite dated by either the fission track (FT) or (U-Th)/He method may give better and more-common correspondence to *z**. In such cases, valuable and nuanced tectonic interpretations may be forthcoming. We do not mean to suggest that dating of modern detrital muscovites is without utility; far from it (see following). However, due to the high T_c of Ar in muscovite, the instances in which one can do things such as calculate basin-wide erosion rates from the range of ages and the range of elevations seem to be the exception rather than the rule (see Braun, 2005).

To test the extent to which the high T_c of Ar in muscovite is to blame for the poor correspondence between ages and hypsometry, we repeated our *t** versus *z** analysis for the FT ages reported by van der Beek et al. (2006) obtained on apatites from three modern river sands from the same areas we are considering using muscovites. These three samples, KAR, MAR10, and MAR6, are from the Karnali basin (essentially the same region as our sample NAG-12), the Marsyandi basin (essentially the same region as sample S24 from Brewer et al., 2006), and the Trisuli basin (essentially the same region as our sample MO-139), respectively. Following the same procedures for the muscovites shown in Figure 6, we compare the *t** and *z** distributions for these apatites in Figure 8; the statistical measures for these distributions are given in Table 3.

The correspondence between *t** and *z** is no better for these samples than for many of the muscovite data shown in Figure 6. The number of grains of apatite analyzed in these samples is far smaller than the muscovite data (n = 32, 54, and 25 for the apatites versus >200 in some muscovites), and it may be that a larger number of apatites could change the *t** distribution such that the *t**-*z** relationships might show a greater similarity, but the available data do not favor the assumptions of Ruhl and Hodges (2005) for even this lower T_c system (~110 °C). It is that case that the closest *t**-*z** relationship among these samples comes from the sample with the smallest catchment area, sample MAR6, from the Marsyandi river, suggesting that there may be some potential for using low-*T* systems to evaluate active tectonics by this approach. It is interesting to note that the statistical comparisons of *t** and *z** for the Marsyandi are similar for muscovite $^{40}Ar/^{39}Ar$ ages (Fig. 6S) and apatite FT ages (Fig. 8A). The low number of grains analyzed and the high uncertainty of individual ages [ranging from 18% to 300% (2σ) of the central age] are in the nature of FT studies on detrital material. A better test of the *t**-*z** approach using a low-T_c system may have to await an application of the U/He approach, which is much less labor intensive (allowing bigger n), and the 2σ on an individual grain is typically less than 10%, compared with the average individual uncertainty of 165% for the apatites reported by van der Beek et al. (2006).

Tectonic Evolution of Nepal

In the new data presented here, two observations stand out with the greatest implications for the large-scale and long-term evolution of the climate and tectonics of the Himalaya. The first is the similarity of the distribution

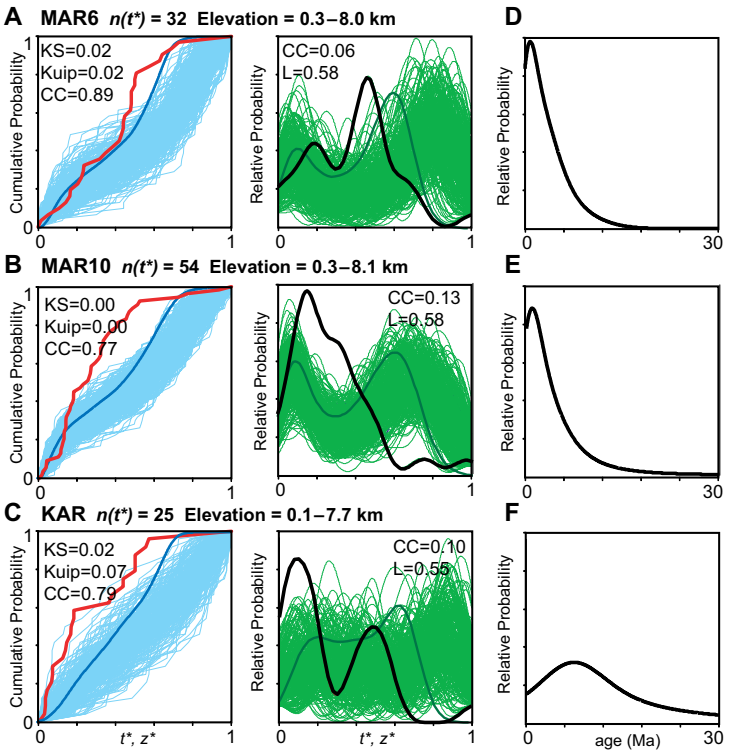

Figure 8. Comparison of *t and *z** (normalized age and normalized topography, respectively) distributions for samples of apatites from modern rivers from van der Beek et al. (2006). A–C follow procedures described in Figure 6. D–F: Nondimensionalized probability density plots (PDP) for apatite fission track ages. Sample numbers are shown. KS—Kolmogorov-Smirnov test; Kuip—Kuiper test. CC—Cross correlation coefficient. L—Likeness. See text for details.**

of $^{40}Ar/^{39}Ar$ ages from muscovites from the modern Karnali River (our sample NAG-12) and the distribution of ages from samples of the Middle Siwalik Group that probably represent a similar geographic source area (Fig. 3D). The second is the dissimilarity of the age distribution of muscovites from the modern Karnali (NAG-12) and the age distribution of muscovites from the modern Narayani (MO-217).

Western Nepal

The similarity of muscovites from the modern and ancient Karnali drainage has potentially important implications for the erosion of the Karnali drainage basin, save for the possibility that the muscovites in sample NAG-12 are mostly recycled from the Middle Siwaliks. Siwalik recycling in the Karnali sediments was reported by Lupker et al. (2012) based on observations on weathering and detrital carbonate signatures. Their observations on sample NAG-12 suggest that this should be limited to less than one-third of the bulk sediment. Nevertheless, we discount the possibility of significant recycling of muscovites based on two lines of reasoning. First, although the location of our sample NAG-12 is south of the outcrop belt of the Siwaliks (Fig. 1), the overwhelming majority of the rocks in the Karnali catchment are other units (mostly LHS and GHS but also part of the TSS and the High Himalayan granites), all of which have significant muscovite content. Therefore, it seems unreasonable that these other units do not contribute most of the muscovite to the modern Karnali, because they make up most of the surface area of the basin. The mixing of 15%–25% of Siwaliks-derived sediments would slightly dilute the ages younger than 5 Ma present in the Narayani, whereas these ages are almost absent in the Karnali. Therefore, the Siwaliks contribution appears insufficient to account for the clear age spectrum between Narayani and Karnali (see following). Because we only chose to analyze grains larger than 333 μm (i.e., medium sand or coarser) we think we would be favoring first-cycle over second-cycle sediments (however, Szulc et al., 2006, analyzed some muscovites from the Siwaliks that were as large as the modern muscovites we report). Based on analysis of FT ages of apatites collected from the Karnali River near our Karnali sample NAG-12, van der Beek et al. (2006, p. 427) concluded that the apatites were "…almost exclusively recycled…" from the Siwaliks. This was based on the similarity between the average age of the 25 apatites analyzed from the modern river (8.1 ± 1.4 Ma) and the average age of the 611 grains analyzed in Siwalik sandstones with stratigraphic ages from 2.8 to 15.9 Ma (7.6 ± 0.4 Ma). We suggest that similarity in average age is not sufficient to conclude similarity in overall distribution and the nature of FT ages on individual grains will smear out PDPs so as to make nuanced comparison problematic (Fig. 8F). van der Beek et al. (2006) further argue for recycling by comparison with the FT apatite ages of Corrigan and Crowley (1990) from Ocean Drilling Program cores from the Bengal Fan ~2000 km to the southeast but, given that the Siwaliks of western Nepal and the modern Karnali River have sampled a much different region than the distal portion of the Bengal Fan, we do not think that this adds any weight to the recycling hypothesis for the modern Karnali. In their discussion, van der Beek et al. (2006, p. 427) noted, "…a modern sediment sample taken upstream of the section and for which Bernet et al. (2006) report detrital ZFT ages would have been able to test [the recycling hypothesis] but unfortunately did not yield sufficient apatite for analysis…" (our brackets). Therefore we conclude that the arguments for significant recycling of muscovites from the Siwaliks in our modern sample are at best equivocal. We do not suggest that our modern sample is free from muscovites derived most recently from outcrops of the Siwalik Group; rather, we suggest the proportion of muscovites in our sample derived from the Siwaliks will be similar to the proportion of the area of the Karnali catchment now covered by the Siwaliks (i.e., small).

Given that the muscovites in the modern Karnali are predominantly not recycled muscovites previously deposited in sandstones of the Siwalik Group, we offer the following hypothesis to explain our current understanding of the

ages of detrital muscovites (this study; DeCelles et al., 2001; Szulc et al., 2006), zircons (Bernet et al., 2006), and apatites (van der Beek et al., 2006) from the modern Karnali and units of the Siwaliks in western Nepal (Fig. 9). Before going into the details of this model, we note that (1) not all muscovites have a T_c for Ar of 400 °C, (2) not all zircons begin to retain fission tracks at 225 °C, (3) the drainage basin of the modern Karnali and its predecessors has evolved in such a way that the source area of the modern river and the rivers that deposited various Siwalik samples from western Nepal are only approximately the same, and (4) the tectonics of western Nepal are clearly more complicated than the one-dimensional model offered here. Notwithstanding these caveats, we think our model is realistic and useful for understanding the available data.

In this model we use data from six primary samples. For muscovite $^{40}Ar/^{39}Ar$ ages, we use our modern sample NAG-12 (n = 204) and sample KZ-7 (n = 150), a sample of the Middle Siwaliks deposited ca. 7 Ma, obtained not far from the NAG-12 sample site reported by DeCelles et al. (2001). Other muscovite data are available from the Karnali section of the Siwaliks (Szulc et al., 2006), but although 478 muscovites were analyzed by $^{40}Ar/^{39}Ar$, these are spread out over 12 samples deposited between 15.9 and 1.0 Ma, such that no samples had more than 83 analyses and some as few as 18. Unfortunately, the samples with the fewest analyses come from the Middle Siwaliks, which are the most relevant to understanding the modern samples. (With n = 18, we can only be 95% confident that we have sampled subsets that make up at least 15% of the total; see Andersen, 2005.) The data from the Middle Siwaliks of Szulc et al. (2006) are consistent with our model but in its formulation we have chosen to focus only on the most robust data, including our modern Karnali sample, the Middle Siwalik sample of DeCelles et al. (2001), and the Lower Siwalik sample of Szulc et al. (2006), K2 (n = 83, detection limit = 3.5%; Andersen, 2005). The other samples used to help us better understand the geologic evolution of western Nepal come from the zircon FT dating reported by Bernet et al. (2006). These zircons come from a Lower Siwaliks sample, KAR-3 (n = 24), a Middle Siwaliks sample, KAR-13 (n = 30, detection limit = 9.5%; Andersen, 2005), and the modern Karnali River, KA-up (n = 64, detection limit = 4.6%; Andersen, 2005). Unfortunately, the Lower Siwaliks were buried to depths at which the fission tracks accumulated in apatites were annealed after Siwalik deposition (van der Beek et al., 2006) and are not useful in understanding the cooling history of the highlands from which these apatites were eroded; therefore, our analysis concentrates on the record revealed by the muscovites and zircons.

For our 1-D model of the tectonic evolution of western Nepal we will consider three adjacent zones within the crust, zone A above zone B above zone C (Fig. 9). Each of these zones have a "thickness" of ~100 °C, or ~3–4 km depending on the geothermal gradient.

We imagine that ca. 22 Ma the center of zone A at ~400 °C, below the nominal closure temperature of Ar in muscovite (Harrison et al., 2009) but all of zones B and C would be at temperatures greater than 400 °C (and, of course, hotter than the zircon partial annealing zone). Thus, most muscovites coming from zone A would have Ar ages older than ca. 21 Ma.

By ca. 16 Ma, zone A has moved to approximately the annealing temperature of fission tracks in zircon (~225 °C, see Bernet and Garver, 2005), the midpoint of zone B is ~400 °C and zone C is essentially completely beneath (hotter than) the closure temperature of Ar in muscovite. This imposes detrital zircon FT (ZFT) ages in zone A of around 18 Ma and Ar ages from muscovite in zone B in the range 18–16 Ma.

By ca. 13 Ma, zone A is at or near the surface, delivering its > 20 Ma muscovites and its ca. 16 Ma zircons to the Lower Siwaliks. In the interval from 16 to 13 Ma, zone B has cooled from temperatures above to temperatures below the ZFT closure temperature (T_c.) Thus the ZFT ages from zone B will be predominantly in this range. Zone C will be on both sides of the ZFT T_c at this time.

Thus, we suggest the rocks now at the surface in western Nepal broadly experienced a cooling of ~200 °C in the interval from ca. 16–13 Ma. Assuming a geothermal gradient of 27 °C/km suggests an erosion rate at the surface of ~2.5 mm/yr during this interval. Although erosion exceeding 2 mm/yr is substantial, it is not out of the question for an active orogen, the Himalaya in particular (e.g., Copeland and Harrison, 1990; Copeland et al., 1990). Although it is difficult to know the shape of the geotherm in the past, it seems to us that if our choice of 27 °C/km is wrong, it is probably too low; higher values of the geothermal gradient would produce lower erosion rates. However, a significant episode of cooling in the middle Miocene for the rocks now at the surface is required to match the primary constraint of the observation that the distribution of Ar muscovite ages for the modern Karnali and the middle Siwaliks are very similar (see following). This interval of rapid erosion would have brought zone A to near the surface in the middle Miocene. This is reflected in the age distribution of muscovites (> 20 Ma, Szulc et al., 2006) and zircons (dominantly 12–20 Ma, Bernet et al., 2006) in the Lower Siwaliks of western Nepal (Fig. 9).

From 13 Ma, our model calls for slower cooling of zones B and C such that zone B is brought to the surface (and consequently eroded into the foreland basin) over the interval from ca. 13–7 Ma. At ~7 Ma the last bits of zone B are exposed and the upper parts of zone C are exposed and making a substantial contribution to the muscovite and zircon populations of the Siwaliks. Thus both the muscovite (DeCelles et al., 2001) and zircon (Bernet et al., 2006) age distributions are dominated by values in the 15–13 Ma range (Fig. 9).

From Middle Siwalik time to the present, erosion in western Nepal must have continued at <1 mm/a, as shown by the continued dominance of middle Miocene ages in the muscovites from the modern Karnali (Figs. 3 and 7) and addition of younger zircons in the modern material compared to the Middle Siwaliks (Bernet et al., 2006). Zone C would have very little variation in muscovite ages but a wide range in zircon ages, thus the dominance of zone C of the material at the surface in our model since Middle Siwalik (Fig. 9).

Thus, we can imagine a one-dimensional model for the thermal history of the Himalayan crust in western Nepal that is consistent with the distribution of detrital zircon FT (ZFT) and muscovite $^{40}Ar/^{39}Ar$ ages in the Siwaliks and modern Karnali, including the key observation that the muscovites in the modern and the Middle Siwaliks are quite similar (Fig. 3D) but the zircons in the same comparison are different. However, such a model must also be tested against

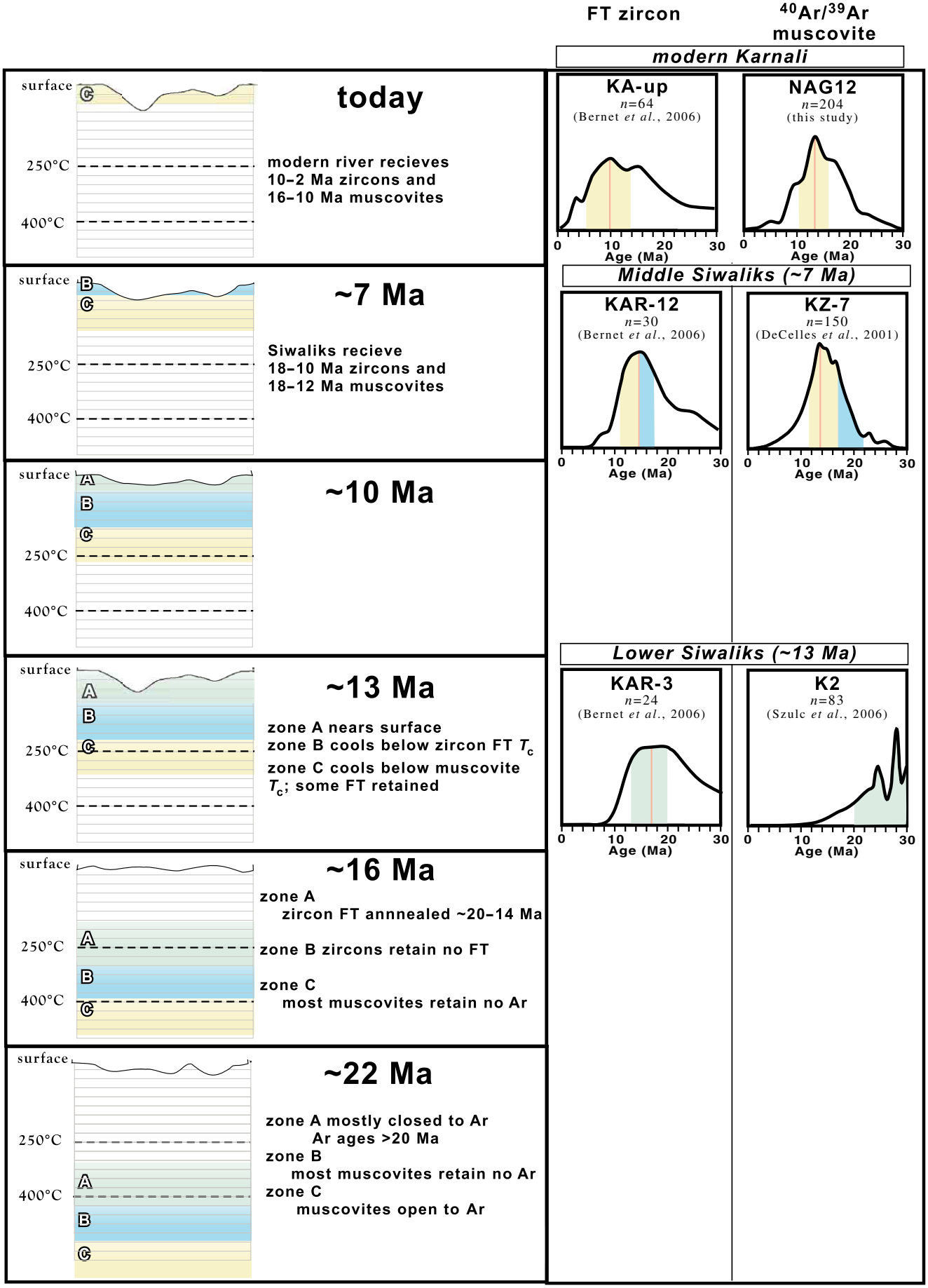

Figure 9. Simple schematic model for the thermal evolution for the rocks of the Karnali River basin. A one-dimensional model for the thermal evolution of three zones of the Himalayan crust is on the left. On the right are the data this model is based on, including the age distributions of zircon fission-track and muscovite $^{40}Ar/^{39}Ar$ ages for samples from the modern Karnali, the Middle Siwalik, and Lower Siwaliks. Colors on the age distribution indicate the dominant zone on the left that was contributing to the population sampled. Red line on age distribution indicates the mode.

the bedrock from which the detrital material is supposed to originate. Owing mostly to the logistics of access, the western part of Nepal has been studied less for thermochronology than the central part of the country, but sufficient detail about the structural evolution of the region is known to test the model presented in Figure 9 (DeCelles et al., 2001; Robinson et al., 2001, 2003; Robinson and Pearson, 2006; Robinson, 2008; Murphy and Copeland, 2005; Pearson and DeCelles, 2005; Robinson and Pearson, 2006; Robinson and McQuarrie, 2012). Essentially all structural models for the evolution of western Nepal include large-scale duplex structures developed over ramps that jump progressively southward over time. Vertical movement over the ramp (when rocks cool rapidly) is followed by significant horizontal movement of many thrust sheets (when they cool slowly or not at all). The closure temperatures we are tracking with muscovite (Ar, ~400 °C) and zircon (FT, ~225 °C), are consistent with mostly horizontally moving thrust sheets since ca. 12 Ma. Robinson and McQuarrie (2012) used the structural modeling of Robinson (2008), sparse thermochronologic data from western Nepal, and the composition and time of deposition of the Siwalik Group to estimate the time and rates of shortening and erosion in western Nepal. They concluded that rates of shortening peaked during the interval from 13 to 10 Ma and erosion peaked in the interval from 11 to 9 Ma, with both the rate of shortening and erosion decreasing since the middle Miocene.

These conclusions are in broad agreement with our one-dimensional model presented in Figure 9, the main difference being that our model suggests the peak of erosion earlier, in the interval 16–13 Ma. These models rely on different sorts of data. The study of Robinson and McQuarrie (2012) used structural and thermochronologic data collected from bedrock in a small number of known locations. The model in Figure 9 uses >500 analyses of muscovite and zircon, but the relative spatial relationships between these minerals at the time they passed through their closure interval is unknowable. Notwithstanding the shortcomings of each of these approaches, the relative similarity of these two models suggests that there is merit in the idea that western Nepal (defined as approximately the Karnali River catchment) underwent an acceleration of erosion through the early Miocene, peaking in the middle Miocene, and slowing since then with rates of erosion averaging <1 mm/yr since ca. 10 Ma (Fig. 9; Robinson and McQuarrie, 2012).

Central Nepal

Because central Nepal is much easier to get to than western Nepal, we have much more bedrock geochronology data from central Nepal with which to compare our detrital data (the same arguments concerning recycling from the Siwaliks applied to sample NAG-12 apply here). Figure 10 shows the outlines of the largest of the drainage basins associated with our samples from central Nepal as well as locations and $^{40}Ar/^{39}Ar$ ages of muscovites from bedrock known to us at the time of this writing. There are 152 bedrock samples, but only 86 of these are from within the Narayani basin. The bedrock samples are far from evenly distributed across the catchment and we can only assume that surface processes have done a good job of averaging the contributions from throughout the basin. At some level of detail we can imagine that sample MO-217, as analyzed, does not faithfully sample all of the bedrock in the catchment because it is biased toward larger muscovites (see preceding). Nevertheless, as shown in Figure 10, there is nothing problematic about the detrital data in light of the bedrock data and vice versa. Because the Kathmandu-Annapurna region has been studied in such detail (thermochronology, metamorphic petrology, structural geology) the detrital muscovites from the greater Narayani basin seem to offer no additional insight other than to predict that areas within the basin yet to be investigated at the same level of scrutiny as the southern flanks of the Annapurna range are unlikely to reveal a geologic history substantially different than that already suggested for this region. Moreover, the broad consistency of the detrital data to the bedrock data in the Narayani basin (where bedrock data are abundant) gives us confidence in our ability to make broad-brush conclusions, based on detrital data, about the tectonic evolution of the Karnali basin (where bedrock data are sparse).

Differences between Western and Central Nepal

The final point we discuss about the new data presented here is the strong dissimilarity between the distribution of the age of muscovites from the modern Karnali drainage and the modern Narayani basin (Fig. 3C). These catchments are about the same size (Table 3) and are adjacent to each other (Fig. 1), but the ages from the Narayani basin to the east (sample MO-217) are distinctly younger than the ages from the Karnali in the west (sample NAG-12). These differences point to distinct histories of erosion in these regions.

We can consider the causes of erosion in the Himalaya over the past 20 m.y. to be of 2 end-member types. No erosion takes place absent the work of wind and water, but in any tectonically active region, such as the Himalaya, the effects of the deformation of the crust can be of equal or much greater importance; rock deformation results in changes in the elevation and relief of the surface, which in turn can influence the location and magnitude of precipitation.

Are the differences in the muscovite ages from the Karnali and the muscovites from the Narayani due to variations in influence of rock deformation (tectonics) or the influence of the work of wind and water (climate) or some combination thereof? We discuss the possible contributions of these two effects in turn.

There is no shortage in the number or range of opinions published on the relative importance of climate versus tectonics to erosion in the Himalaya. These include that climate is more important than tectonics in the northwestern Himalaya since the Pliocene (Bookhagen et al., 2005a, 2005b; Thiede et al., 2005), that records of exhumation in the northwestern Himalaya are poorly correlated with modern-day rainfall, relief, and stream power (Thiede et al., 2009), that tectonics are more important than climate in central Nepal (Burbank et al., 2003; Blythe et al., 2007; Godard et al., 2014), that climate is more important than tectonics in central Nepal (Wobus et al., 2003; Huntington et al.,

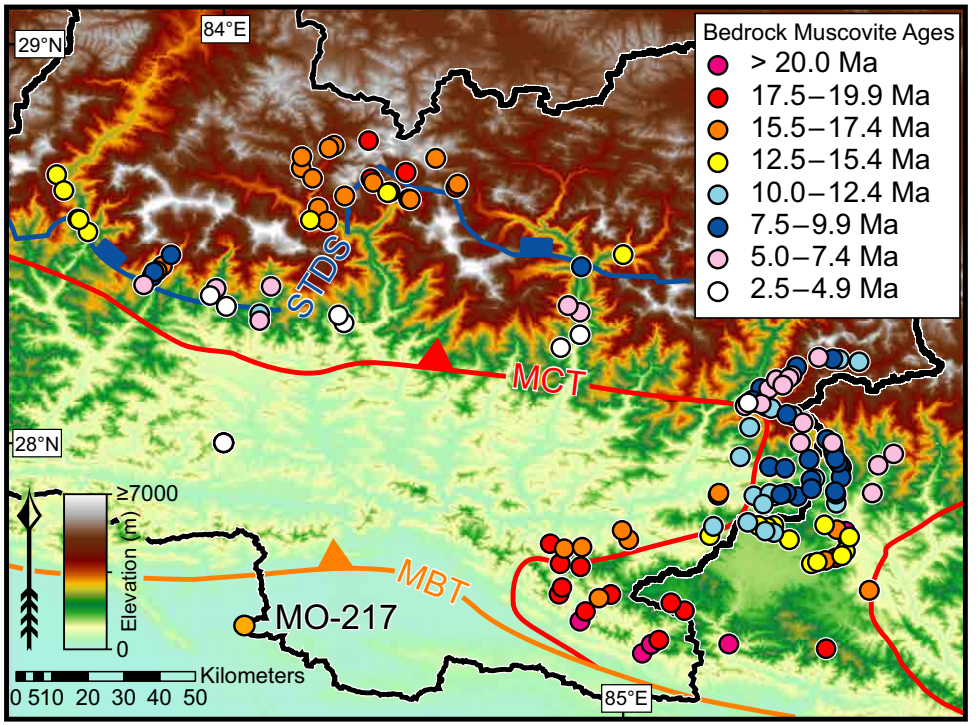

Figure 10. Colored circles show location and $^{40}Ar/^{39}Ar$ muscovite age from basement samples (data from Copeland et al., 1990, 1991; Godin et al., 2001, 2006; Herman et al., 2010; Martin et al., 2014). MBT—Main Boundary thrust; MCT—Main Central thrust; STDS—South Tibetan Detachment system.

2006), that climate is more important than tectonics in Bhutan (Grujic et al., 2006), that tectonics are more important than climate in Bhutan (Adlakha, et al., 2013a), and that there is a feedback between the work of wind and water and rock deformation, each influencing the other (Avouac and Burov, 1996; Hodges et al., 2004; Adlakha et al., 2013b).

We have already established that the tectonics of western Nepal (broadly coincident with the Karnali basin), or at least the vertical component of tectonic movement, may be characterized by a lessening of intensity since ca. 10 Ma. Research suggests that a similar lessening did not occur in central Nepal. Herman et al. (2010) suggested that a midcrustal duplex initiated in the Kathmandu region ca. 10 Ma, leading to an increase of uplift rate at front of the High Himalaya from ~1 to >3 mm/yr. Much of the area modeled by Herman et al. (2010) is within the Narayani basin. Several other studies have concluded that the MCT underwent significant reactivation in the late Miocene (Harrison et al., 1997; Catlos et al., 2001; Kohn et al., 2001; Wobus et al., 2003). Not all of these studies are compatible with each other; it is not our point here to suggest so, but rather to note that several lines of evidence have been marshaled to argue for recent tectonism in the Narayani basin. Whereas in western Nepal there seems to be evidence for a lessening of tectonic activity since ca. 10 Ma, the area just to the east in central Nepal was characterized by an acceleration of tectonic activity during the same period.

In order for these two contiguous regions to maintain this disparate erosional history, if rock deformation is the reason, there must be some tectonic boundary that can preferentially partition rock deformation to the Narayani basin relative to the Karnali basin. Murphy et al. (2014) identified a structure that could explain the variation in the erosional history in central Nepal and western Nepal (see Fig. 3C); they suggested that the western Nepal fault system (WNFS) is a series of faults that form a >350-km-long zone of active dextral shear that links the MFT in the southeast to the Karakoram fault in the northwest (Fig. 11A). This is consistent with models of the southeastward propagation of the Karakoram fault (Murphy et al., 2000; Murphy and Copeland, 2005).

This fault system does not match precisely the boundary between the two modern drainage basins, but ~95% of the Narayani basin and 39% of the Karnali basin are to the east of the WNFS and 5% of the Narayani basin and 61% of the Karnali basin are to the west of the WNFS (Fig. 11A). If the WNFS operates as described by Murphy et al. (2014), it could be an effective boundary that would explain the difference in erosional history to the west and east of this line. Murphy et al. (2014) did not speculate as to the time of initiation of the WNFS,

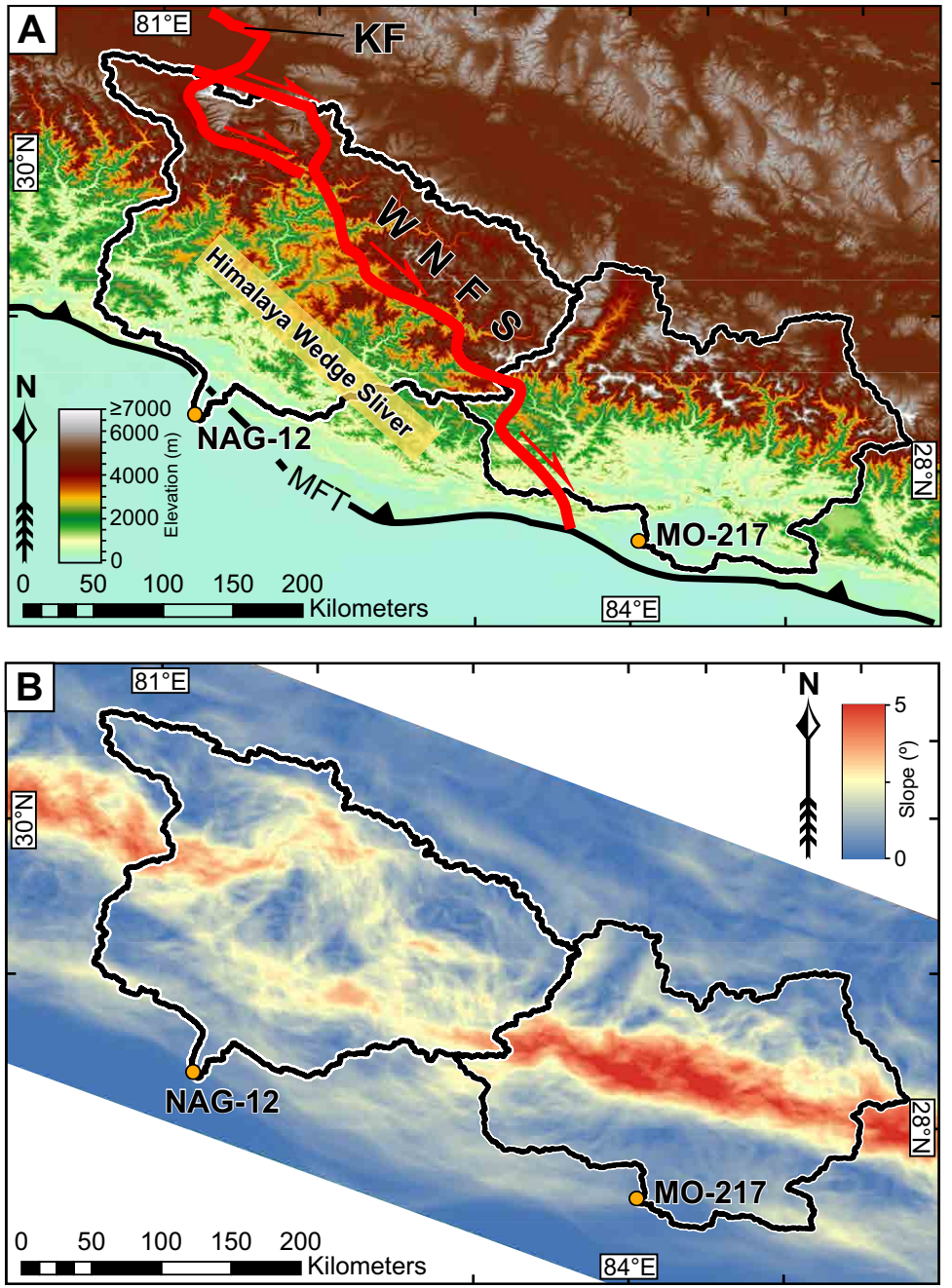

Figure 11. (A) Map of the study area showing the drainage basins of samples NAG-12 and MO-217. WNFS—western Nepal fault system of Murphy et al. (2014); MFT—Main Frontal thrust; KF—Karakoram fault. (B) Map of slope of mean elevation (calculated using a moving window of 5 km radius) taken from Harvey et al. (2015) with drainage basins of samples NAG-12 (Karnali River) and MO-217 (Narayani River) superimposed.

but studies in northwest Nepal and adjacent territory in Tibet suggest that the southeastward migration of the Karakoram fault across the Himalaya began in the middle to late Miocene (Murphy et al., 2000; Murphy and Copeland, 2005). This could explain the slowing of tectonic activity in the Karnali basin since ca. 10 Ma with much of this drainage being placed in the Himalayan wedge sliver of Murphy et al. (2014); to the west of the WNFS, deformation is partitioned into an orogen-normal component and an orogen-parallel component, whereas to the east the deformation is largely orogen normal. However, this model would place the northeast portion of the Karnali catchment east of the WNFS, presumably facilitating rock deformation and erosion in this area. However, the paucity of muscovite $^{40}Ar/^{39}Ar$ ages younger than 10 Ma in sample NAG-12 and the sample from the Middle Siwaliks (DeCelles et al., 2001) might cause some to argue that the throughgoing strain partitioning described by Murphy et al. (2014) could not have been established as early as 10 Ma, and some other (or at least an additional) explanation for the differences in the muscovite age distributions from the Karnali and the Narayani basins must be found.

Harvey et al. (2015) noted geomorphic variations between central Nepal and western Nepal with the both the parameters slope of mean elevation and smoothed relief being generally smaller in the west. We reproduce their map of the slope of mean elevation for central and western Nepal and superimpose the drainage basins associated with our samples NAG-12 and MO-217 in Figure 11B. This shows that the drainage divide between the Karnali and Narayani basins has a strong correspondence to where the average slope of the Himalayan front decreases significantly (this can also be seen in the topographic profiles of Figs. 1B–1E). It is perhaps not remarkable that the slope of topography within a given drainage basin would not have much variation in either absolute magnitude or spatial variability, but it is tempting to regard the geomorphic differences between the basins shown in Figure 11B to reflect mostly recent differences. Harvey et al. (2015, p. 517) suggested that "…the topographic … discontinuity from central to western Nepal is the result of a recent southward stepping of the midcrustal ramp along the Main Himalayan thrust.." from the north to the south. Harvey et al. (2015) did not quantify what they meant by "recent" but it seems clear from their discussion that this hypothesis does not extend into the past more than 1 or 2 m.y. However, the muscovite data presented here suggest that erosion in the modern Karnali and Narayani basins has been different since ca. 10 Ma or earlier.

Whereas thermochronologic data (especially from high T_c systems such as muscovite) give insight into erosion that must span millions of years, the cosmogenic isotope ^{10}Be can be used to assess basin-wide rates of erosion over roughly millennial time scales. Studies of this sort in the Karnali and Naryani basins (Lupker et al., 2012; Godard et al., 2014) suggest broadly similar rates of erosion in the two basins. Recycling of Siwalik sediments may, however, bias this observation for the Karnali basin. One sample taken upstream of the MBT returns an erosion rate of 0.6 mm/yr, significantly lower than those of the Narayani (1.3–2.1 mm/yr) or downstream Karnali (1–2.4 mm/yr) basins. In the Narayani basin, there is little correlation between the ^{10}Be-derived erosion rates and modern rainfall (Godard et al., 2014).

Bookhagen and Burbank (2010) analyzed the satellite-derived TRMM-2B31 data obtained from 1997 to 2007 to better understand the modern pattern of rainfall in the Himalaya. They found that at elevations <500 m above sea level (asl) there is a strong gradient in annual rainfall with as much as six times more rain in eastern India than in Pakistan; this is a reflection of the track of the Asian monsoon, which moves in the summer from the Bay of Bengal westward. The effect of the Asian monsoon was thought to drop off significantly west of the Sutlej valley by Bookhagen and Burbank (2010) and west of the Ganges valley, 150 km to the east, by Barros et al. (2004); either of these transition zones is far west of the Karnali and Narayani basins. However, at elevations greater than 500 masl, Bookhagen and Burbank (2010, p. 15 of 25) found no significant variation in annual rainfall along strike of the Himalaya; they found that "…spatially averaged annual rainfall rates appear to be almost uniform along the Himalaya with a slight westward-decreasing gradient with annual averages between 1.5 and 2.0 m/yr." A large proportion of both the Karnali and Narayani basins today is above 500 m. When evaluating the reasons for erosion in orogenic belts, the isolation of the effects of the work of wind and water apart from the effects of rock deformation is made difficult by the brief interval over which relevant meteorological data are available. That notwithstanding, we note there seems to be little correlation between the spatial distribution of rainfall during the interval 1997–2007 and the distribution of $^{40}Ar/^{39}Ar$ ages from muscovites in the Karnali and Narayani drainages.

Based on thermochronology from three locations spanning ~750 km along the arc of the Himalaya [the Garhwal Himalaya of India, the Marsyandi drainage in central Nepal (a portion of the Narayani basin), and the Mount Everest area in eastern Nepal], Huntington et al. (2006, p. 107), seeing "…no evidence for important changes in the far-field tectonics of the Himalayan-Tibetan orogenic system…" concluded that the change in cooling rate in these locations ca. 2 Ma was a result of climate change. A variety of evidence argues for late Pliocene global climate change (e.g., Raymo, 1994; Maslin et al., 1998; Peizhen et al., 2001; Zhisheng et al., 2001; Gupta and Thomas, 2003), but if forces from above (climate) and not forces from below (rock deformation) are responsible for the changes in cooling rates discussed by Huntington et al. (2006), one would expect the area between the Garhwal Himalaya in India and the Marsyandi region of central Nepal to contain similar coercion toward the climate hypothesis. This is because of the nature of climate being broad rather than localized. The Karnali basin occupies ~300 of the 500 km that separate the Garhwal and Marsyandi regions along the Himalayan arc. The Narayani basin (which includes the Marsyandi) shows abundant evidence for accelerating post-Miocene erosion, but much available evidence argues against this for the Karnali basin (see preceding). Two adjacent regions with such different erosion histories are inconsistent with the climate-dominant hypothesis for Himalayan exhumation.

When comparing the modern Karnali and Narayani basins, we see a difference in the distribution of $^{40}Ar/^{39}Ar$ ages of detrital muscovites >333 μm in diameter (this study), a difference in average slope and relief (Harvey et al., 2015), a similarity in the rate of erosion over a millennial scale (Lupker et al., 2012; Godard et al., 2014), and a similarity in rainfall above 500 m elevation

from 1997 to 2007 (Bookhagen and Burbank, 2010). This suggests that variation of the kind seen in both Figures 2C and 11B must be the consequence of long-term variation that cannot be smoothed out by similar amounts of rainfall (at least over the past few millennia).

Therefore, because of the time necessary to produce the difference in muscovite cooling ages (Fig. 2C) and because of the side by side juxtaposition of basins with significant geomorphic variation (Figs. 1 and 11B), we conclude that it has been predominantly localized forces from below (strain partitioning) rather than regional forces from above (climate) that were responsible for the differences in erosional history of the Karnali and Narayani basins.

CONCLUSIONS

In central and western Nepal, there is generally poor correspondence between the normalized distribution of topography (z^*) and the normalized distribution of $^{40}Ar/^{39}Ar$ ages of detrital muscovites (t^*) from modern rivers. This suggests that even in small basins, the modern hypsometry cannot be used to as a tool to understand the cooling history of the bedrock of the basin when using relatively high T_c systems in active orogens.

The comparison of modern detrital thermochronology from the Karnali River in western Nepal to similar data from Miocene sedimentary rocks from the same region broadly suggests a thermal history for western Nepal consistent with vigorous tectonics (and attendant erosion) before the middle Miocene, but a significant diminution in the rate of erosion since ca. 10 Ma.

The $^{40}Ar/^{39}Ar$ ages of detrital muscovites from the Narayani basin in central Nepal suggest a markedly different history with an acceleration of the rate of erosion since ca. 10 Ma.

There is little variation in modern precipitation or millennial-scale rates of erosion based on cosmogenic isotopes between the Karnali and Narayani basins. Because these two basins are adjacent, it seems inappropriate to explain the significant differences in erosional history (as evidenced by the ages of modern detrital muscovites) with a mechanism that operates on a broad scale (variation of climate). If climate change were the reason for the acceleration of erosion in the Narayani basin, we would expect to see much more of a signal of this effect in the neighboring Karnali basin. We therefore conclude that the main reason for the difference in erosional history of the two basins is strain partitioning within the Himalaya. The work of wind and water has an important role to play in the shaping of the landscape, but it appears that in the Nepali Himalaya, forces from below (tectonics) play a stronger role in the erosional history of the orogeny than forces from above (climate).

ACKNOWLEDGMENTS

We thank Cristina Urizar for help in the laboratory, Jon Harvey for sharing his geographic information system data, Matthias Bernet for help in evaluating his zircons, and Peter van der Beek for help with his apatites. Support on this project for Bertrand was supplied by Lavoisier grant 5635/SUR/UFF from the French Ministry of Foreign Affairs. This work was improved by reviews from van der Beek, Lang Farmer, and an anonymous reviewer.

REFERENCES CITED

Adlakha, V., Lang, K.A., Patel, R.C., Lal, N., and Huntington, K.W., 2013a, Rapid long-term erosion in the rain shadow of the Shilong Plateau, eastern Himalaya: Tectonophysics, v. 582, p. 76–83, doi:10.1016/j.tecto.2012.09.022.

Adlakha, V., Patel, R.C., and Lal, N., 2013b, Exhumation and its mechanism: A review of exhumation studies in the Himalaya: Geological Society of India Journal, v. 81, p. 481–502, doi:10.1007/s12594-013-0064-0.

Andersen, T., 2005, Detrital zircons as tracers of sedimentary provenance: limiting conditions from statistics and numerical simulation: Chemical Geology, v. 216, p. 249–270, doi:10.1016/j.chemgeo.2004.11.013.

Avouac, J.P., and Burov, E.B., 1996, Erosion as a driving mechanism of intracontinental mountain growth: Journal of Geophysical Research, v. 101, no. B8, p. 17,747–17,769, doi:10.1029/96JB01344.

Barros, A.P., Kim, G., Williams, E., and Nesbitt, S.W., 2004, Probing orographic controls in the Himalayas during the monsoon using satellite imagery: Natural Hazards and Earth System Sciences, v. 4, p. 29–51, doi:10.5194/nhess-4-29-2004.

Bernet, M., and Garver, J.I., 2005, Fission-track analysis of detrital zircon, *in* Reiners, P.W., and Ehlers, T.A., eds., Low-temperature thermochronology: Techniques, interpretations, and applications: Mineralogical Society of America Reviews in Mineralogy and Geochemistry Volume 58, p. 205–238.

Bernet, M., van der Beek, P., Pik, R., Huyghe, P., Mugnier, J.-L., Labrin, E., and Szulc, A., 2006, Miocene to recent exhumation of the central Himalaya determined from combined detrital zircon fission-track and U/Pb analysis of Siwalik sediments, western Nepal: Basin Research, v. 18, p. 393–412, doi:10.1111/j.1365-2117.2006.00303.x.

Blythe, A.E., Burbank, D.W., Schmidt, C.K., and Putkonen, J., 2007, Plio-Quaternary exhumation history of the central Nepalese Himalaya: 1. Apatite and zircon fission track and apatite [U-Th]/He analyses: Tectonics, v. 26, TC3002, doi:10.1029/2006TC001990.

Bollinger, L., Avouac, J.P., Beyssac, O., Catlos, E.J., Harrison, T.M., Grove, M., Goffe, B., and Sapkota, S., 2004, Thermal structure and exhumation history of the Lesser Himalaya in central Nepal: Tectonics, v. 23, TC5015, doi:10.1029/2003TC001564.

Bookhagen, B., and Burbank, D.W., 2010, Towards a complete Himalayan hydrologic budget: Spatiotemporal distribution of snowmelt and rainfall and their impact on river discharge: Journal of Geophysical Research, v. 115, F03019, doi:10.1029/2009JF001426.

Bookhagen, B., Thiede, R.C., and Strecker, M.R., 2005a, Late Quaternary intensified monsoon phases control landscape evolution in the northwest Himalaya: Geology, v. 33, p. 149–152, doi:10.1130/G20982.1.

Bookhagen, B., Thiede, R.C., and Strecker, M.R., 2005b, Abnormal monsoon years and their control on erosion and sediment flux in the high, arid northwest Himalaya: Earth and Planetary Science Letters, v. 231, p. 131–146, doi:10.1016/j.epsl.2004.11.014.

Braun, J., 2005, Quantitative constraints on the rate of landform evolution derived from low-temperature thermochronology, *in* Reiners, P.W., and Ehlers, T.A., eds., Low-temperature thermochronology: Techniques, interpretations, and applications: Mineralogical Society of America Reviews in Mineralogy and Geochemistry Volume 58, p. 351–374.

Brewer, I.D., 2005, Detrital-mineral thermochronology: Investigations of orogenic denudation in the Himalaya of central Nepal [Ph.D. thesis]: State College, Pennsylvania State University, 198 p.

Brewer, I.D., Burbank, D.W., and Hodges, K.V., 2003, Modeling detrital cooling-age populations: insights from two Himalayan catchments: Basin Research, v. 15, p. 305–320, doi:10.1046/j.1365-2117.2003.00211.x.

Brewer, I.D., Burbank, D.W., and Hodges, K.V., 2006, Downstream development of a detrital cooling-age signal: Insights from $^{40}Ar/^{39}Ar$ muscovite thermochronology in the Nepalese Himalaya, *in* Willett, S.D., et al., eds., Tectonics, climate and landscape evolution: Geological Society of America Special Paper 398, p. 321–388. doi:10.1130/2006.2398(20).

Burbank, D.W., Blythe, A.E., Putkonen, J., Pratt-Sitaula, B., Gabet, E., Oskin, M., Barros, A., and Ojha, T.P., 2003, Decoupling of erosion and precipitation in the Himalayas: Nature, v. 426, p. 652–655, doi:10.1038/nature02187.

Catlos, E.J., Harrison, T.M., Kohn, M.J., Grove, M., Ryerson, F.J., Manning, C.E., and Upreti, B.N., 2001, Geochronologic and thermobarometric constraints on the evolution of the Main Central Thrust, central Nepal Himalaya: Journal of Geophysical Research, v. 106, p. 16,177–16,204, doi:10.1029/2000JB900375.

Cattin, R., and Avouac, J.-P., 2000, Modeling mountain building and the seismic cycle in the Himalaya of Nepal: Journal of Geophysical Research, v. 105, p. 13,389–13,407, doi:10.1029/2000JB900032.

Coleman, M.E., and Hodges, K.V., 1995, Evidence for Tibetan plateau uplift before 14 Myr ago from a new minimum age for east-west extension: Nature, v. 374, p. 49–52, doi:10.1038/374049a0.

Coleman, M.E., and Hodges, K.V., 1998, Contrasting Oligocene and Miocene thermal histories from the hanging wall and footwall of the South Tibetan detachment in the central Himalaya from $^{40}Ar/^{39}Ar$ thermochronology, Marsyandi Valley, central Nepal: Tectonics, v. 17, p. 726–740, doi:10.1029/98TC02777.

Copeland, P., and Harrison, T.M., 1990, Episodic rapid uplift in the Himalaya revealed by $^{40}Ar/^{39}Ar$ analysis of detrital K-feldspar and muscovite, Bengal Fan: Geology, v. 18, p. 354–357, doi:10.1130/0091-7613(1990)018<0354:ERUITH>2.3.CO;2.

Copeland, P., Harrison, T.M., Kidd, W.S.F., Xu Ronghua, and Zhang Yuquan, 1987, Rapid early Miocene acceleration of uplift in the Gangdese belt, Xixang, southern Tibet, and its bearing on the accommodation mechanisms of the India-Asia collision: Earth and Planetary Science Letters, v. 86, p. 240–252, doi:10.1016/0012-821X(87)90224-X.

Copeland, P., Harrison, T.M., and Heizler, M.T., 1990, $^{40}Ar/^{39}Ar$ single-crystal dating of detrital muscovite and K-feldspar from Leg 116, southern Bengal Fan: Implications for the uplift and erosion of the Himalaya, *in* Cochran, J.R., and Stowe, D.A.W., eds., Proceedings of the Ocean Drilling Program, Scientific Results, Volume 116: College Station, Texas, Ocean Drilling Program, p. 93–114, doi:10.2973/odp.proc.sr.116.119.1990.

Copeland, P., Harrison, T.M., Hodges, K.V., Maréujol, P., Le Fort, P., and Pêcher, A., 1991, An early Pliocene thermal disturbance of the Main Central Thrust, central Nepal: Implications for Himalayan tectonics: Journal of Geophysical Research, v. 96, p. 8475–8500, doi:10.1029/91JB00178.

Corrigan, J.D., and Crowley, K.D., 1990, Fission-track analysis of detrital apatites from Sites 717 and 718, Leg 116, Indian Ocean, *in* Cochran, J.R., and Stowe, D.A.W., eds., Proceedings of the Ocean Drilling Program, Scientific Results, Volume 116: College Station, Texas, Ocean Drilling Program, p. 75–92, doi:10.2973/odp.proc.sr.116.118.1990.

DeCelles, P.G., Robinson, D.M., Quade, J., Ojha, T.P., Garzione, C.N., and Copeland, P., 2001, Stratigraphy, structure, and tectonic evolution of the Himalayan fold-thrust belt in western Nepal: Tectonics, v. 20, p. 487–509, doi:10.1029/2000TC001226.

Gabet, E.J., Burbank, D.W., Pratt-Sitaula, B., Putkonen, J., and Bookhagen, B., 2008, Modern erosion rates in the High Himalayas of Nepal: Earth and Planetary Science Letters, v. 267, p. 482–494, doi:10.1016/j.epsl.2007.11.059.

Godard, V., Bourles, D.L., Spinabella, F., Burbank, D.W., Bookhagen, B., Fisher, G.B., Moulin, A., and Léanni, L., 2014, Dominance of tectonics over climate in Himalayan denudation: Geology, v. 42, p. 243–246, doi:10.1130/G35342.1.

Godin, L., Parrish, R.R., Brown, R.L., and Hodges, K.V., 2001, Crustal thickening leading to exhumation of the Himalayan metamorphic core of central Nepal: Insight from U-Pb geochronology and $^{40}Ar/^{39}Ar$ thermochronology: Tectonics, v. 20, p. 729–747, doi:10.1029/2000TC001204.

Godin, L., Gleeson, T.P., Searle, M.P., Ullrich, T.D., and Parrish, R.R., 2006, Locking of southward extrusion in favour of rapid crustal-scale buckling of the Greater Himalayan sequence, Nar valley, central Nepal, *in* Law, R.D., et al., eds., Channel flow, ductile extrusion and exhumation in continental collision zones: Geological Society of London Special Publication 268, p. 269–292, doi:10.1144/GSL.SP.2006.268.01.13.

Grujic, D., Coutand, I., Bookhagen, B., Bonnet, S., Blythe, A., and Duncan, C., 2006, Climate forcing of erosion, landscape, and tectonics in the Bhutan Himalayas: Geology, v. 34, p. 801–804, doi:10.1130/G22648.1.

Gupta, A.K., and Thomas, E., 2003, Initiation of Northern Hemisphere glaciation and strengthening of the northeast Indian monsoon: Ocean Drilling Program Site 758, eastern equatorial Indian Ocean: Geology, v. 31, p. 47–50, doi:10.1130/0091-7613(2003)031<0047:IONHGA>2.0.CO;2.

Harrison, T.M., Ryerson, F.J., LeFort, P., Yin, A., Lovera, O.M., and Catlos, E.J., 1997, A late Miocene–Pliocene origin for the Central Himalayan inverted metamorphism: Earth and Planetary Science Letters, v. 146, p. E1–E7, doi:10.1016/S0012-821X(96)00215-4.

Harrison, T.M., Grove, M., Lovera, O.M., and Catlos, E.J., 1998, A model for the origin of Himalayan anatexis and inverted metamorphism: Journal of Geophysical Research, v. 103, p. 27,017–27,032, doi:10.1029/98JB02468.

Harrison, T.M., Célérier, J., Aikman, A.B., Hermann, J., and Heizler, M.T., 2009, Diffusion of ^{40}Ar in muscovite: Geochimica et Cosmochimica Acta, v. 73, p. 1039–1051, doi:10.1016/j.gca.2008.09.038.

Harvey, J.E., Burbank, D.W., and Bookhagen, B., 2015, Along-strike changes in Himalayan thrust geometry: Topographic and tectonic discontinuities in western Nepal: Lithosphere, v. 7, doi:10.1130/L444.1 (in press).

Herman, F., et al., 2010, Exhumation, crustal deformation and thermal structure of the Nepal Himalaya derived from the inversion of thermochronological and thermobarometric data and modeling of the topography: Journal of Geophysical Research, v. 115, B06407, doi:10.1029/2008JB006126.

Hodges, K.V., Wobus, C., Ruhl, K., Schildgen, T., and Whipple, K., 2004, Quaternary deformation, river steepening, and heavy precipitation at the front of the Higher Himalayan ranges: Earth and Planetary Science Letters, v. 220, p. 379–389, doi:10.1016/S0012-821X(04)00063-9.

Huntington, K.W., and Hodges, K.V., 2006, A comparative study of detrital mineral and bedrock age-elevation methods for estimating erosion rates: Journal of Geophysical Research, v. 111, F03011, doi:10.1029/2005JF000454.

Huntington, K.W., Blythe, A.E., and Hodges, K.V., 2006, Climate change and late Pliocene acceleration of erosion in the Himalaya: Earth and Planetary Science Letters, v. 252, p. 107–118, doi:10.1016/j.epsl.2006.09.031.

Johnson, M.R.W., and Rogers, G., 1997, Rb-Sr ages of micas from the Kathmandu complex, central Nepalese Himalaya: Implications for the evolution of the main central thrust: Geological Society of London Journal, v. 154, p. 863–869, doi:10.1144/gsjgs.154.5.0863.

Kohn, M., Catlos, E.J., Ryerson, F.J., and Harrison, T.M., 2001, Pressure-temperature-time path discontinuity in the Main Central thrust zone, central Nepal: Geology, v. 29, p. 571–574, doi:10.1130/0091-7613(2001).

Lupker, M., Blard, P.-H., Lavé, J., France-Lanord, C., Leanni, L., Puhol, N., Charreau, J., and Bourlès, D., 2012, ^{10}Be-derived Himalayan denudation rates and sediment budgets in the Ganga basin: Earth and Planetary Science Letters, v. 333–334, p. 146–156, doi:10.1016/j.epsl.2012.04.020.

Martin, A.J., Copeland, P., and Benowitz, J.A., 2014, Muscovite $^{40}Ar/^{39}Ar$ ages help reveal the Neogene tectonic evolution of the southern Annapurna Range, central Nepal, *in* Mukherjee, S., et al., eds., Tectonics of the Himalaya: Geological Society of London Special Publication 412, p. 199–220, doi:10.1144/SP412.5.

Maslin, M.A., Li, X.S., Loutre, M.-F., and Berger, A., 1998, The contribution of orbital forcing to the progressive intensification of Northern Hemisphere glaciation: Quaternary Science Reviews, v. 17, p. 411–426, doi:10.1016/S0277-3791(97)00047-4.

McDougall, I., and Harrison, T.M., 1999, Geochronology and thermochronology by the $^{40}Ar/^{39}Ar$ method (second edition): New York, Oxford University Press, 269 p.

Murphy, M.A., and Copeland, P., 2005, Transtensional deformation in the central Himalaya and its role in accommodating growth of the Himalayan orogeny: Tectonics, v. 24, TC4012, doi:10.1029/2004TC001659.

Murphy, M.A., Yin, A., Kapp, P., Harrison, T.M., Lin, D., and Jinghui, G., 2000, Southward propagation of the Karakoram fault system, southwest Tibet: Timing and magnitude of slip: Geology, v. 28, p. 451–454, doi:10.1130/0091-7613(2000)28<451:SPOTKF>2.0.CO;2.

Murphy, M.A., Taylor, M.H., Gosse, J., Silver, C.R.P., Whipp, D.M., and Beaumont, C., 2014, Limit of strain partitioning in the Himalaya marked by large earthquakes in western Nepal: Nature Geoscience, v. 7, p. 38–42, doi:10.1038/ngeo2017.

Pearson, O.N., and DeCelles, P.G., 2005, Structural geology and regional tectonic significance of the Ramgarh thrust, Himalayan fold-thrust belt of Nepal: Tectonics, v. 24, TC4008, doi:10.1029/2003TC001617.

Peizhen, Z., Molnar, P., and Downs, W.R., 2001, Increased sedimentation rates and grain sizes 2–4 Myr ago due to the influence of climate change on erosion rates: Nature, v. 410, p. 891–897, doi:10.1038/35073504.

Raymo, M.E., 1994, The initiation of Northern Hemisphere glaciation: Annual Review of Earth and Planetary Sciences, v. 22, p. 353–383, doi:10.1146/annurev.ea.22.050194.002033.

Reiners, P.W., Ehlers, T.A., Mitchell, S.G., and Montgomery, D.R., 2003, Coupled spatial variations in precipitation and long-term erosion rates across the Washington Cascades: Nature, v. 426, p. 645–647, doi:10.1038/nature02111.

Robinson, D.M., 2008, Forward modeling the kinematic sequence of the central Himalayan thrust belt, western Nepal: Geosphere, v. 4, p. 785–801, doi:10.1130/GES00163.1.

Robinson, D.M., and McQuarrie, N., 2012, Pulsed deformation and variable slip rates within the central Himalayan thrust belt: Lithosphere, v. 4, p. 449–464, doi:10.1130/L204.1.

Robinson, D.M., and Pearson, O.N., 2006, Exhumation of Greater Himalayan rock along the Main Central thrust, Nepal: Implications for channel flow, *in* Law, R.D., et al., eds., Channel flow, extrusion, and exhumation in continental collision zones: Geological Society of London Special Publication 268, p. 255–268, doi:10.1144/GSL.SP.2006.268.01.12.

Robinson, D.M., DeCelles, P.G., Patchett, P.J., and Garzione, C.N., 2001, The kinematic evolution of the Nepalese Himalaya interpreted from Nd isotopes: Earth and Planetary Science Letters, v. 192, p. 507–521, doi:10.1016/S0012-821X(01)00451-4.

Robinson, D.M., DeCelles, P.G., Garzione, C.N., Pearson, O.N., Harrison, T.M., and Catlos, E.J., 2003, Kinematic model for the Main Central thrust in Nepal: Geology, v. 31, p. 359–362, doi:10.1130/0091-7613(2003)031<0359:KMFTMC>2.0.CO;2.

Ruhl, K.W., and Hodges, K.V., 2005, The use of detrital mineral cooling ages to evaluate steady state assumptions in active orogens: An example from the central Nepalese Himalaya: Tectonics, v. 24, TC4015, doi:10.1029/2004TC001712.

Satkoski, A.M., Wilkinson, B.H., Hietpas, J., and Sampson, S.D., 2013, Likeness among detrital zircon populations—An approach to the comparison of age frequency data in time and space: Geological Society of America Bulletin, v. 125, p. 1783–1799, doi:10.1130/B30888.1.

Schelling, D., and Arita, K., 1991, Thrust tectonics, crustal shortening, and the structure of the far eastern Nepal Himalaya: Tectonics, v. 10, p. 851–862, doi:10.1029/91TC01011.

Simon-Labric, T., Brocard, G.Y., Teysseier, C., van der Beek, P.A., Reiners, P.W., Shuster, D.L., Murray, K.E., and Whitney, D.L., 2014, Low-temperature thermochronologic signature of range-divide migration and breaching in the North Cascades: Lithosphere, v. 6, p. 473–482, doi:10.1130/L382.1.

Szulc, A.G., et al., 2006, Tectonic evolution of the Himalaya constrained by detrital ^{40}Ar-^{39}Ar, Sm-Nd and petrographic data from the Siwalik foreland basin succession, SW Nepal: Basin Research, v. 18, p. 375–391, doi:10.1111/j.1365-2117.2006.00307.x.

Thiede, R.C., Arrowsmith, J.R., Bookhagen, B., McWilliams, M.O., Sobel, E.R., and Strecker, M.R., 2005, From tectonically to erosionally controlled development of the Himalayan orogeny: Geology, v. 33, p. 689–692, doi:10.1130/G21483.1.

Thiede, R.C., Ehlers, T.A., Bookhagen, B., and Strecker, M.R., 2009, Erosional variability along the northwest Himalaya: Journal of Geophysical Research, v. 114, F01015, doi:10.1029/2008JF001010.

van der Beek, P., Robert, X., Mugnier, J.-L., Bernet, M., Huyghe, P., and Labrin, E., 2006, Late-Miocene–recent exhumation of the central Himalaya and recycling in the foreland basin assessed by apatite fission-track thermochronology of Siwalik sediments, Nepal: Basin Research, v. 18, p. 413–434, doi:10.1111/j.1365-2117.2006.00305.x.

Vannay, J.C., and Hodges, K.V., 1996, Tectonometamorphic evolution of the Himalayan metamorphic core between the Annapurna and Dhaulagiri, central Nepal: Journal of Metamorphic Geology, v. 14, p. 635–656, doi:10.1046/j.1525-1314.1996.00426.x.

Vermeesch, P., 2004, How many grains are needed for a provenance study?: Earth and Planetary Science Letters, v. 224, p. 441–451, doi:10.1016/j.epsl.2004.05.037.

Whipple, K.X., 2009, The influence of climate on the tectonic evolution of mountain belts: Nature Geoscience, v. 2, p. 97–104, doi:10.1038/ngeo413.

Wobus, C.W., Hodges, K.V., and Whipple, K.X., 2003, Has focused denudation sustained active thrusting at the Himalayan topographic front?: Geology, v. 31, p. 861–864, doi:10.1130/G19730.1.

Wobus, C.W., Heimsath, A., Whipple, K.X., and Hodges, K.V., 2005, Active out-of-sequence thrust faulting in the central Nepalese Himalaya: Nature, v. 434, p. 1008–1011, doi:10.1038/nature03499.

Zhisheng, A., Kutzbach, J.E., Prell, W.L., and Porter, S.C., 2001, Asian monsoons and phased uplift of the Himalaya-Tibetan plateau since late Miocene times: Nature, v. 411, p. 62–66, doi:10.1038/35075035.